Degradation Mechanisms of Electrodes Promotes Direct Regeneration of Spent Li-Ion Batteries: A Review

Kai Jia [#, a], Guorui Yang[#, a], Yujia He [a], Zhenjiang Cao [a], Juntao Gao [a], Hongyang Zhao [a] Zhihong Piao [b], Junxiong Wang [b,c], Amr. M. Abdelkader [e], Zheng Liang [c], R. Vasant Kumar [d], Guangmin Zhou *[, b], Shujiang Ding*[, a], Kai Xi *[, a]

a Department of Applied Chemistry, School of Chemistry, Engineering Research Center of Energy Storage Materials and Devices, Ministry of Education, National Innovation Platform (Center) for Industry-Education Integration of Energy Storage Technology, State Key Laboratory for Electrical Insulation and Power Equipment, Xi'an Jiaotong University, Xi'an 710049, China

b Tsinghua Shenzhen International Graduate School &Tsinghua-Berkeley Shenzhen Institute (TBSI), Tsinghua University, Shenzhen 518055, China

c Frontiers Science Center for Transformative Molecules, School of Chemistry and Chemical Engineering, Shanghai Jiao Tong University, Shanghai 200240, China

d Department of Materials Science and Metallurgy, University of Cambridge, 27 Charles Babbage Road, Cambridge CB3 0FS, United Kingdom

e Faculty of Science and Technology, Bournemouth University, Poole House, Talbot Campus, Poole, Dorset BH12 5BB, United Kingdom

* Corresponding authors: Guangmin Zhou (Email: guangminzhou@sz.tsinghua.edu.cn), Shujiang Ding (Email: dingsj@mail.xjtu.edu.cn), Kai Xi (Email: kx210.cam@xjtu.edu.cn)

# These authors were equal major contributors.

Abstract

The rapid growth of electric vehicle use is expected to cause a significant environmental problem in the next few years due to the large number of spent lithium-ion batteries (LIBs). Recycling spent LIBs wouldn't only alleviate the environmental problems but also address the challenge of limited natural resources shortages. While several hydro- and pyrometallurgical processes have been developed for recycling different components of spent batteries, direct regeneration presents clear environmental and economic advantages. The principle of the direct regeneration approach is restoring the electrochemical performance by healing the defective structure of the spent materials. Thus, the development of direct regeneration technology largely depends on the formation mechanism of defects in spent LIBs. This review systematically detailed the degradation mechanisms and types of defects found in diverse cathode materials, graphite anodes, and current collectors during the battery's lifecycle. Building on this understanding, we've outlined principles and methodologies for directly rejuvenating materials within spent LIBs. We also propose the main challenges and solutions for the large-scale direct regeneration of spent LIBs. Furthermore, this review aims to pave the way for the direct regeneration of materials in discarded lithium-ion batteries by offering a theoretical foundation and practical guidance.

Key words: Spent LIBs, direct regeneration, target repair, degradation mechanism, recycling methods.

Introduction

With the rapid increase in demand for electrical vehicles (EVs), the number of EVs on roads expected to reach 7.5 million globally by 2030. [1] Most EVs currently use lithium-ion batteries (LIBs) as the main power source. However, the service life of the state-of-the-art LIBs ranged between 5-8 years, implying that numerous retired LIBs will be produced in the future. [2,3] It is projected that by 2030, the global total capacity of exhausted LIBs will surpass 104 GWh. [4] Spent LIBs contain large amounts of valuable metal elements, such as Co, Ni, and Li,[5] that have limited natural resources. Also, extracting raw materials of these elements puts significant pressure on the supply chain processes due to several geo-political issues. If these spent LIBs are not managed appropriately, it is a great waste of resources, which is contrary to the social subject of sustainable development. Additionally, the heavy metal elements contained in spent LIBs are toxic, which pollutes the environment and, more importantly, will eventually reach the human body through the enrichment of the biological chain and affect people's health. [6] Therefore, these spent LIBs must be recycled in a green and efficient way, many governments have issued relevant policies (Figure 1a) for battery recycling.[7-37]

In LIBs, approximately 40% of the overall battery cost can be attributed to cathode materials, and the core of recycling spent LIBs revolves around the recovery of these cathode materials. [38] Currently, the traditional methods to recycle spent cathode materials are hydrometallurgical and pyrometallurgical. [39-42] Guo et al. have made improvements to traditional battery recycling methods and proposed a mild and more efficient strategy for extracting precious metals through the selection of suitable solvents. [43, 44]. However, these methods still have several drawbacks. First, the traditional recovery of cathode materials requires extreme conditions, such as strong acid or high temperature, to destroy the structure of the spent cathode, where secondary pollution and high energy consumption are inevitable.[45] Secondly, these methods cannot make full use of the energy stored in the spent cathodes, in which there is still about 80% residual capacity.[46] Third, the routine of hydrometallurgical and pyrometallurgical regeneration is extremely cumbersome because it includes multiple

extraction, separation, purification, and resynthesis steps. [47,48]

From this perspective, direct recycling technology has emerged as a compelling alternative to traditional recycling techniques. The direct recycling method is a green, milder recycling method compared to the traditional recycling methods. This mixes the pretreated spent cathodes with Li salt, followed by a calcination step to obtain regenerated cathode materials with restored or even improved electrochemical performance. [49] Direct recycling of spent cathodes does not require excessive energy and environmental costs; the process is simple and utilizes energy efficiently. [50,51] Many studies have shown that direct recycling yields higher economic benefits than traditional recycling methods. [2,49,52,53] The most critical advantage of direct recycling over hydrometallurgical and pyrometallurgical recycling is that it does not cause damage to the structure of the spent cathode during the regeneration. Recently, the United States Department of Energy built the LIB Recycling Center (ReCell), with the objective of implementing direct recycling practices that reuse of all components from spent LIBs, achieving a closed-loop manufacturing process for LIB recycling. [1]

The primary method of direct regeneration of spent LIBs is the targeted repair of defects in failed materials and the restoration of the materials' structures before cycling the battery. Therefore, designing the repair strategy depends largely on understanding the degradation mechanisms and defective types of failed materials. Based on recent research results, we comprehensively and systematically summarized the defect formation mechanisms, types, and characterization methods for spent materials. Namely, we investigate the failure of $LiCoO_2$ (LCO), $LiNi_xCo_yMn_zO_2$ (x+y+z=1), $LiFePO_4$ (LFP), $LiMn_2O_4$ (LMO) cathode materials, graphite negative electrode, and Al and Cu current collectors. The article then moves to critically analysing the technology thus far developed for directly repairing targeted defects in spent positive and negative electrodes. Finally, we discuss the existing challenges of direct recycling and offer potential solutions to overcome them.

An overview of battery recycling policies for different countries and union

Japan:

Influenced by raw materials, Japan has been a leader in recycling spent batteries and basic, comprehensive, and special laws have regulated battery recycling. In 1991, the Law for Promotion of Utilization of Recyclable Resources was enacted, which further specified the specific channels for recycling used batteries from consumers to recycling enterprises, clarified the responsibilities and obligations of producers, managers, consumers, and other links, and stipulated that producer are strictly responsible for recycling batteries. [8] After the successful implementation of the battery recycling program in 1994, the establishment of the power battery "production-sales-recycling" recycling system, clearly defined the battery manufacturer as the main recycling body, through automobile dealers, gas stations, retailers, and other channels to carry out waste battery recycling. [9] In 2000, the Law for Promotion of Effective Utilization of Resources was enacted, which aims to establish a sound material cycle economy through a series of measures, such as its requirement to reduce, reuse and recycle (3Rs) as part of measures covering the upstream sector, including product design, to the downstream sector (e.g., collection and recycling of used and end-of-life products). [12,13] In 2018, a number of Japanese automakers formed the Battery Recycling Alliance (represented by Toyota, Honda, etc.) to promote the recycling of decommissioned power batteries for electric vehicles. This manufacturer-based recycling model enables companies to develop and design batteries with greater consideration for their sustainability at the source and improves the subsequent recycling rate.

Europe:

In Europe, there are a number of frameworks for battery recycling, and several framework directives related to power batteries have been issued since 1991, [7,16,18,19] which have gradually improved the battery recycling system. In 2023, the European Union issued Regulation Concerning Batteries and Waste Batteries (EU) 2023/1542, amending Directives 2008/98/EC and 22019/1020, and replacing and repealing the former Batteries Directive 2006/66/EC. [36] The law requires that all batteries placed on

the EU market be subject to full life cycle management to promote the sustainable and recyclable development of the EU battery industry. The EU Battery Regulation has set a new environmental benchmark for the sustainable development of the global battery and new energy vehicle industries with its proposed supply chain due diligence requirements, battery carbon footprint, minimum recyclable battery material targets, and restrictions on toxic and hazardous substances.

United States:

The United States regulates used batteries at three levels: federal, state, and local. The three levels of law complement and regulate each other, thus making the U.S. battery recycling legal system perfect. Currently, there are two federal laws related to lithium battery recycling, one is the Mercury-Containing and Rechargeable Battery Management Act, [10] which requires companies and stores that sell lead-acid and nickel-metal hydride batteries to accept and recycle used batteries, [11] and the other is the Resource Conservation and Recovery Act (RCRA), which sets the regulatory framework for dealing with non-hazardous and hazardous solid waste. California enacted AB-2407 Recycling: Lithium-Ion Vehicle Batteries: Advisory Group in 2018, which proposes to establish an advisory group by April 2019 and provide policy recommendations by April 2020 to ensure that 90 percent of the state's discarded lithium electric vehicle batteries are recycled safely and economically. [25,26] In 2021, the U.S. proposed National Blueprint for Lithium Batteries 2021-2030, which emphasizes the establishment of a complete and competitive lithium battery recycling value chain in the U.S. to achieve the end-of-life reuse of lithium batteries and the large-scale recycling of key raw materials and will introduce more federal recycling policies in 2025. [31] In November of 2021, the Infrastructure Investment and Jobs Act of 2021 was enacted, which includes electric vehicles and recycling of battery processing materials, with a $5 billion investment in this area. [33] The Inflation Reduction Act of 2022 specifies that all electric vehicle battery materials recycled in the United States, regardless of source, are considered American-made and eligible for subsidies. [34]

Korea:

Since the end of the 20th century, Korea has been enacting and revising special

laws and regulations on the recycling of e-waste, such as the Act on the Promotion of Saving and Recycling Resources, which was implemented in 2002, and initially set up a system for the return of deposits for the disposal of waste. [13,14] In 2003, the Act on the Promotion of Saving and Recycling Resources was comprehensively revised, and the Extended Producer Responsibility (EPR) system was introduced. [15] Based on the EPR recycling system, researchers have also proposed a battery recycling system for Korea, where battery manufacturers set up producer responsibility organizations to coordinate the costs associated with the recycling of power batteries, and the government promotes the transfer of batteries from consumers to government-designated recycling centers through subsidies, and materials companies obtain metals through dismantling and recycling and return them to manufacturers or importers, thus forming a good battery recycling cycle. The South Korean government proposed the K-Battery Development Strategy in 2021, which plans to invest 40.6 trillion won in the power battery sector by 2030 to ensure South Korea's dominance in the global battery industry. [32] This strategic initiative increases investment in the battery industry, builds Korea's local battery ecosystem and promotes the localization of the battery supply chain, driving domestic demand growth in the local battery market. As part of South Korea's strategy, South Korea's major battery manufacturers, including LG New Energy, Samsung, SK Innovation, and other well-known companies, have recently made frequent moves in the power battery recycling market, in the form of purchasing shares of companies specializing in this field and other forms of layout.

China:

In order to protect the environment, improve the utilization rate of resources, implement the scientific outlook on development, and realize sustainable socio-economic development, the Ministry of Ecology and Environment of the People's Republic of China issued a technical policy for the recycling of automotive products in 2006. [17] The purpose of this policy is to guide the production and sale of automobiles, and mobilize the relevant enterprises to Develop and promote the recycling of end-of-life automotive products. With the massive growth in battery recycling in 2016, China enacted a series of regulations and related policies. [20-24,27-30,35,37] The main objectives

of China's policy system for battery recycling, especially power battery recycling for new energy vehicles, are to promote resource recycling, environmental protection, and the healthy development of the industry. Implementation Plan of Extended Producer Responsibility System imposes extended producer responsibility for battery recycling. [20] Vehicle Power Battery Recycling Utilization Energy Detection (GB/T34015-2017) provides for the determination of the appearance, polarity, voltage, charging and discharging current, and residual energy of storage batteries. [23] The Code for Recycling and Dismantling of Vehicle Power Batteries (GB/T33598-2017) provides for safety measures, procedures, storage, and management of vehicle batteries. [24] The Pilot Work on Recycling and Utilization of Power Batteries for Electric Vehicles clarifies pilot areas and enterprises for battery recycling. [27] Guidelines for Construction and Operation of New Energy Vehicle Power Battery Recycling Service Outlets narrow definitions for battery recycling facilities (other than those for lead-acid batteries). [30] In order to increase the comprehensive utilization management of used new energy vehicle power batteries, promote resource recycling, and promote the high-quality development of the new energy vehicle industry, the Ministry of Industry and Information Technology (MIIT) will accelerate the development of the Administrative Measures for the Recycling of Power Storage Batteries for New Energy Vehicles, [37] which is an improvement of the standard system of the power battery.

Recycling process

The schematic of recycling spent LIBs is shown in Figure 1b. Before recycling, or regenerating, in general, spent batteries need to be fully discharged, and the discharge process is usually carried out in a salt solution (NaCl, $NaSO_4$, etc.). After discharge, the batteries are mechanically disassembled or crushed. For pyrometallurgical recovery (Figure 1b), the crushed samples are directly subjected to high-temperature treatment, where the separators, binders, conductive agents, graphite negative electrodes, and electrolytes contained in spent LIBs are all removed. The Al current collector can be a reducing agent to reduce transition metals and form corresponding alloys. The alloys are then subjected to several leaching, separating and purifying steps to obtain the target element in the leaching liquid. Finally, these metals can be converted into precursors

for synthesizing cathode materials of LIBs. Regenerated cathode materials for LIBs can be obtained by sintering the mixture of precursors and LiOH. While a number of pyrometallurgical techniques have demonstrated encouraging results, their high-temperature requirements make them energy-intensive and contribute to CO_2 emissions. For hydrometallurgical recycling (Figure 1b), the plastic, separator, battery shell, cathode materials, and negative electrode graphite contained in spent LIBs are separated through several physical beneficiation steps. The separated positive electrode materials are leached with an acid or alkali, and then the corresponding metal salt is obtained by further separation, purification, and other processes. The corresponding metal salt is then utilized to create the cathode materials. The hydrometallurgical recovery process involves the use of acid/alkali solutions, which inevitably leads to secondary environmental pollution. In addition, its recycling steps are tedious. The challenges of the pyro- and hydro-metallurgical processes magnify for cathode materials with minimum or no Co content, such as rich nickel and $LiFePO_4$ from economic benefits.

The attenuated performance of cathode materials is primarily attributed to the Li loss and the changes in crystal structure it brings. Therefore, effective Li replenishment for cathode materials can repair the electrode and restore its performance to the level of freshly-made cathode materials. The direct regeneration of cathode materials directly supplements Li to the cathode materials via appropriate methods (solid state sintering, electrochemical, deep eutectic solvent, solution, and other strategies) to obtain directly usable cathode materials (Figure 1b). From the above analysis, it can be seen that the direct regeneration method has a simple operating process, less environmental pollution, and greater value and income compared to traditional pyrometallurgical and hydrometallurgical recycling methods, which makes the direct recycling method attract more and more attention.

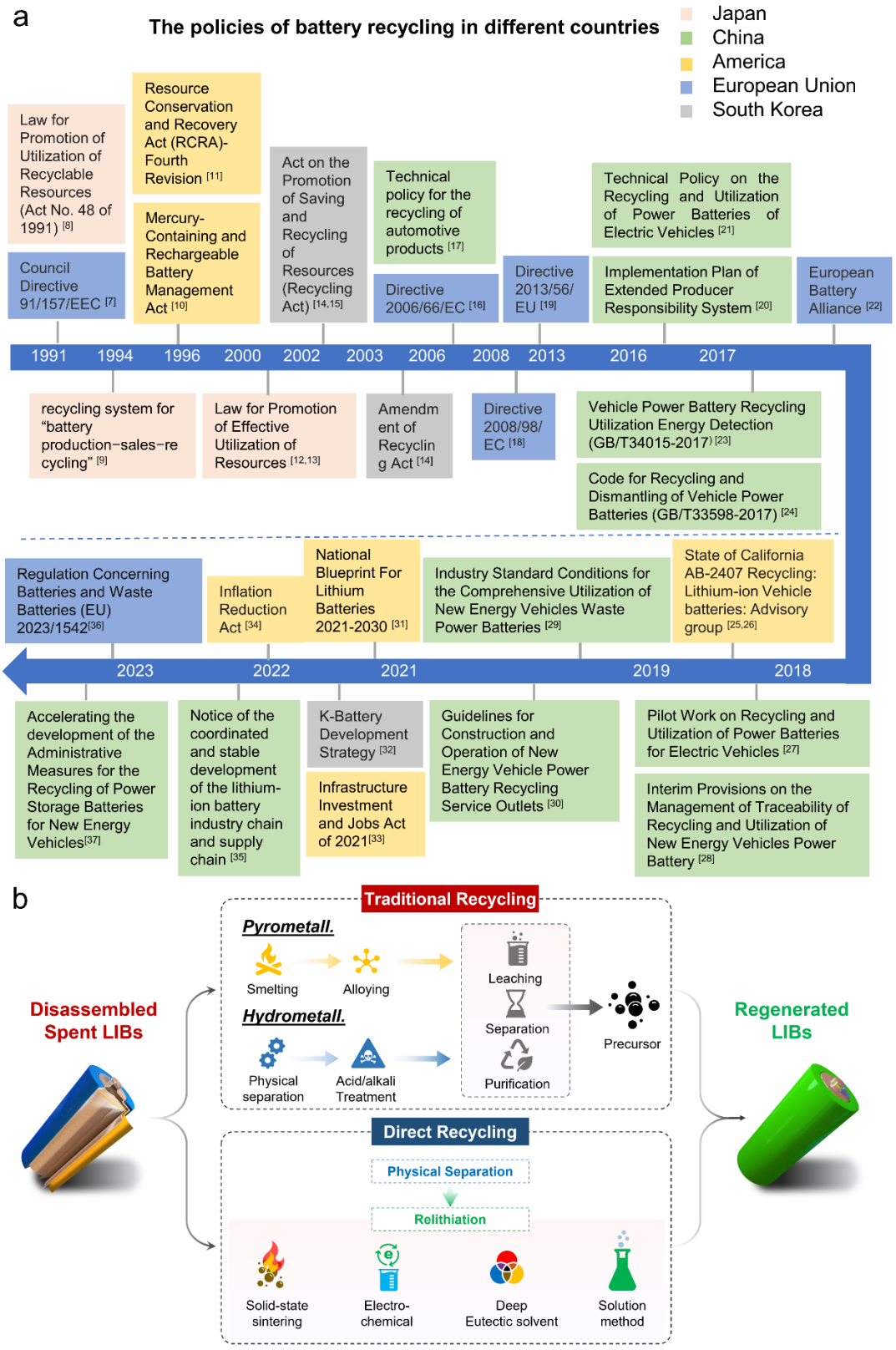

Figure 1. (a) The policies of battery recycling in different countries. (b) Schematic of pyrometallurgical, hydrometallurgical, and direct recycling processes.

Since the types and intensity of defects plays a significant role in the regeneration

processes, we have systematically summarized the defects generated during cycling (including the corresponding characterization methods) and further illustrated the degradation mechanisms of materials during cycling. Taking the spent layered cathodes as an example, their degradation degree is related to the Li vacancies, which cause changes in the chemical binding between the transition metal and the spacing of the (003) crystal plane in the layered cathode. The degradation level (Figure 2a) of spent cathode materials can be characterized by X-ray diffraction (XRD), inductively coupled plasma (ICP), Fourier transform infrared (FTIR), Raman spectroscopy and some other spectroscopic techniques. The degradation mechanisms of cathode materials, the types of surface macroscopic defects (cracks/void/hole), and formed microscopic atomic level defects (spinel/rock salt) during its cycle can be explored by scanning electron microscopy (SEM), focused ion beam (FIB)-SEM, energy dispersive spectrometer (EDS), time-of-flight secondary ion mass spectrometry (TOF-SIMS), high-resolution transmission electron microscopy (HRTEM), electron energy loss spectroscopy (EELS), X-ray photoelectron spectroscopy (XPS), atomic force microscopy (AFM), and synchrotron radiation (Figure2a). Based on an adequate understanding of the formed defects and degradation mechanisms of spent electrode materials, we have summarized in Figure 2b the recycling methods (mainly including solid state sintering, electrochemical, molten salt or deep eutectic solvent, solution-based, and ionic liquid-based) for different spent cathode materials. Specifically, due to researchers' insufficient understanding of the degradation mechanisms of spinel LMO, the solution-based Li replenishment method and solid-state sintering are currently available for the regeneration of spent LMO. Therefore, there are other methods worth exploring for the direct regeneration of spent LMO. In the following sections, we will conduct a detailed analysis of degradation mechanisms, generated defect types of the cycled cathodes (LCO, $LiNi_xCo_yMn_zO_2$ (x+y+z=1), LFP, LMO) and negative (graphite) materials and current collectors (Al and Cu), and recycling methods of aforementioned spent materials in LIBs.

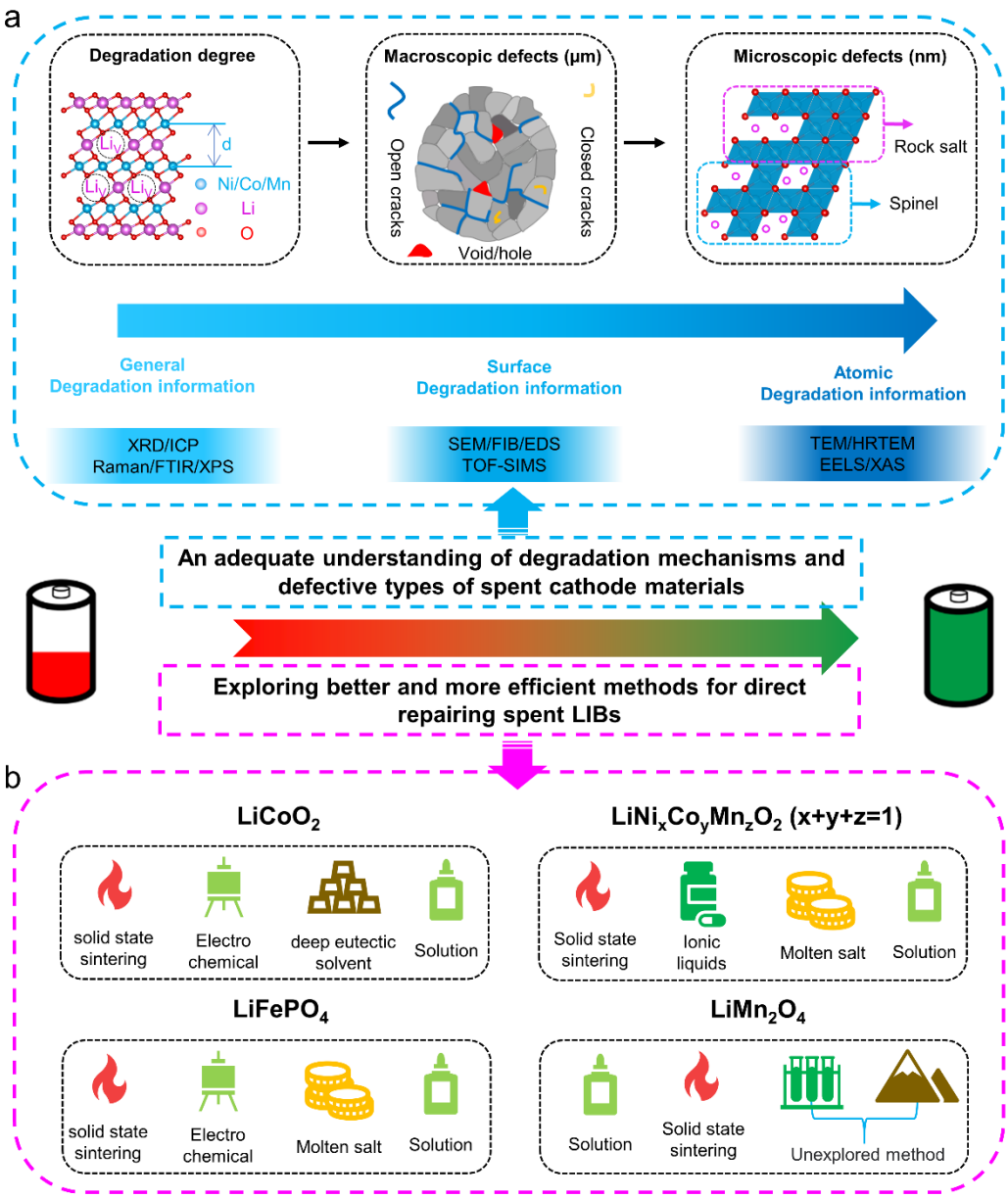

Figure 2. (a) The explored process of degradation mechanism of the spent cathodes. (b) Direct recycling methods of different cathode materials.

We have compiled an overview of the main functionalities, uniqueness, and limitations in the typical characterization methods employed for examining the defective structures within spent cathodes (Table 1).

In terms of functionalities, XRD/XRD Rietveld Refinement/Raman Spectroscopy/ XPS/ICP analysis provide general information on defect structures within spent cathodes. Meanwhile, SEM/FIB-SEM/AFM offer insights into the defect structures at the micrometer or sub-micrometer scale in spent cathodes. And, TEM/EELS/XANES furnish atomic-level information regarding defect structures. The specific uniqueness

and limitations of the above characterization methods are summarized in Table 1 in detail.

Table 1. An overview of the main functionalities, uniqueness, limitations in the typical characterization methods employed for examining the defective structures in spent cathodes.

characterization technique	Main function	Uniqueness	Limitations
XRD	XRD can qualitatively assess the degree of degradation in cathode materials; determine the formed impurity phase in the cathode material after failure.	XRD can be used for in situ studies of structural transformations in materials during charging and discharging processes.	For spent cathodes, there is a limited capability for microscale analysis.
XRD Rietveld Refinement	XRD Rietveld Refinement can quantitatively analyze the concentration of anti-site defects and the number of lithium vacancies in spent cathodes; it also enables the determination of unit cell parameters.	XRD pattern full fitting produces reliable results.	For complex microstructures such as short-range ordering, local defects, and interfacial structures, XRD Rietveld refinement may not provide detailed local information.
ICP	Quantitative analysis of different elemental concentrations	Simultaneous analysis of multiple elements with high sensitivity and low detection limits (mg/L).	Requires a large amount of sample; the sample is dissolved during testing, and completely destroying its structure.
Raman	Investigation of vibrational characteristics of chemical bonds between transition metals and non-metallic lements.	Raman is a non-destructive testing technique.	Raman can only provide information about the surface of the cathodes

XPS	XPS is used for analyzing the valence states of elements and the composition of chemical bonds in cathode materials.	XPS has an extremely high sensitivity in analyzing surface elements of failed cathodes and can also determine the relative abundances of different chemical states of the same element.	Limited depth profiling capability; insufficient sensitivity for detecting light elements; limited spatial resolution (10 um).
SEM	Observation of cracks or pores on the surface of spent cathode materials.	High-resolution imaging (with magnification up to 100,000 times).	SEM only reveals defect structures on the surface of the spent cathode material.
AFM	Observation of surface undulations caused by lattice slips on spent cathode materials.	It has nanoscale resolution.	Imaging speed is relatively slow; particularly, when acquiring high-magnification images, the scanning speed can be significantly reduced.
FIB-SEM	Observation of internal cracks or pores within spent cathode materials.	FIB allows for precise cutting at sub-micron or even nano-scale levels, while SEM provides real-time imaging simultaneously.	A significant amount of heat are generated during cutting, leading to structural deformation.

TEM	Observation of defect structures at the nanoscale in spent cathodes.	TEM offers extremely high spatial resolution, reaching the atomic level.	Compared to other specialized chemical analysis methods, TEM has limited capacity for obtaining detailed chemistry information.
EELS	Analysis of the chemical states of elements at various positions (within the nanoscale range).	EELS accurately determines the energy loss of electrons as they traverse a sample, enabling the disclosure of the presence and chemical states of various elements within the sample, including details such as oxidation states, valences, and coordination environments.	EELS signals are typically weak and require longer integration times and higher detector sensitivities.
XANES	Analyzing valence state information and coordination environments of elements in failed cathodes.	XANES can reveal atomic-level structural details without necessitating reliance on long-range ordered crystal structures.	The quantitative analysis of XANES data is complex due to the calculation of absorption coefficients involves multi-body effects and multiple scattering.

Degradation mechanisms of LCO and corresponding characterization methods

LCO is widely used in portable electronics. The defects of spent LCO mainly include the formation of Co_3O_4 on the surface and the Li vacancies formed in the subsurface and core of LCO during cycling. [54] In this section, the formation process of the failure structure of LCO and the corresponding characterization methods for defects will be discussed.

The XRD characterizations of spent LCO and regenerated LCO were performed by Dong et al. The XRD diffraction spectrum of spent LCO in Figure 3a showed the Co_3O_4 impurity phase relative to the diffraction peak of pristine LCO (JCPDS no. 75-0532).[55] During extended cycling, the formation of Co_3O_4 defects occurs due to the migration of Co atoms from the transition metal layer to the Li layer within the structure of the material, [56,57] and the Co_3O_4 failed structure is generally located on the outer surface of spent LCO. More detailed structural analyses are discussed later. There is also a clear shift in the diffraction peak at ~19° for the spent LCO relative to that of regenerated material (DR-LCO, DR-D-0.5%, DR-D-1%, DR-D-2%) at different repair conditions (Figure 3b). This shift was attributed to the formation of Li vacancies in spent LCO. The generation of Li vacancies changes the electrostatic repulsion force between non-metallic element O of the (003) crystal face in the LCO lattice structure. [58,59] Consequently, the lattice spacing of the (003) crystal plane in spent LCO is observed to be marginally larger compared to that of its fresh or unaltered counterpart. Zhang et al. quantified the concentration of Li vacancies and the proportion of the Co_3O_4 impurity phase (Figure 3c) in spent LCO by the Rietveld refined XRD. [60] Yan et al. found that obvious Li depressed on the surface of the cycled samples with different cycling conditions, which was the reason for the formation of Co_3O_4 on the surface of the failed cathode materials (Figure 3d-f)[61]. XPS has also been employed to investigate the chemical states of Co_3O_4 defects present on the surface of spent LCO. Dong et al. found that the content of Co^{2+} and Co^{3+} are relatively similar for spent LCO, [55] and Co^{3+}content is much greater than Co^{2+}content in regenerated LCO. Increasing the Co^{2+} content is related to the formation of Co_3O_4 on the surface of LCO during cycling. Here,

Co_3O_4 can be regarded as a composite of CoO (Co^{2+}) and Co_2O_3 (Co^{3+}). In-situ Raman spectroscopy serves as a potent analytical tool for elucidating the structural transformations undergone by cathode materials both during and subsequent to the charging/discharging cycles. In the case of LCO, the A_{1g} mode detected at approximately 594 cm^{-1} signifies the lattice vibrations associated with Co-O stretching, while the E_g mode appearing near 488 cm^{-1} corresponds to the O-Co-O bending modes. The characteristic peaks at 700 cm^{-1} are associated with the formation of Co_3O_4. [62,63] Cheng et al. demonstrated that LCO produces the failed structure Co_3O_4 (Figure 3g) during cycling, [64] and its formation is connected with the release of lattice oxygen from the cathode material. The ICP analysis can qualitatively determine the degree of degradation of spent cathodes. Cheng et al. calculated the molar ratio of Li/Co of cathode materials at different states of charge. [65] The results showed the molar ratio of Li/Co in spent LCO was 0.795, 0.827, and 0.853 at different discharge capacities (7.6, 15.1, and 64.4 mAh/g) in the first cycle. After regeneration, the molar ratio of Li/Co of the cathode material recovered to 0.998, 0.993, and 0.997 (Figure 3h). Spent cathode materials exhibiting defects demonstrated significantly reduced discharge capacities along with inferior cycling capabilities. However, upon regeneration, the electrochemical properties of the regenerated cathode materials were found to be comparable to those of their original counterparts. (Figure 3i). They also present that the concentration of Li vacancies in spent LCO is significantly correlated with the residual capacity of spent LCO, [40] where the lower the residual capacity of the spent cathode, the more Li vacancies are contained (Figure 3j).

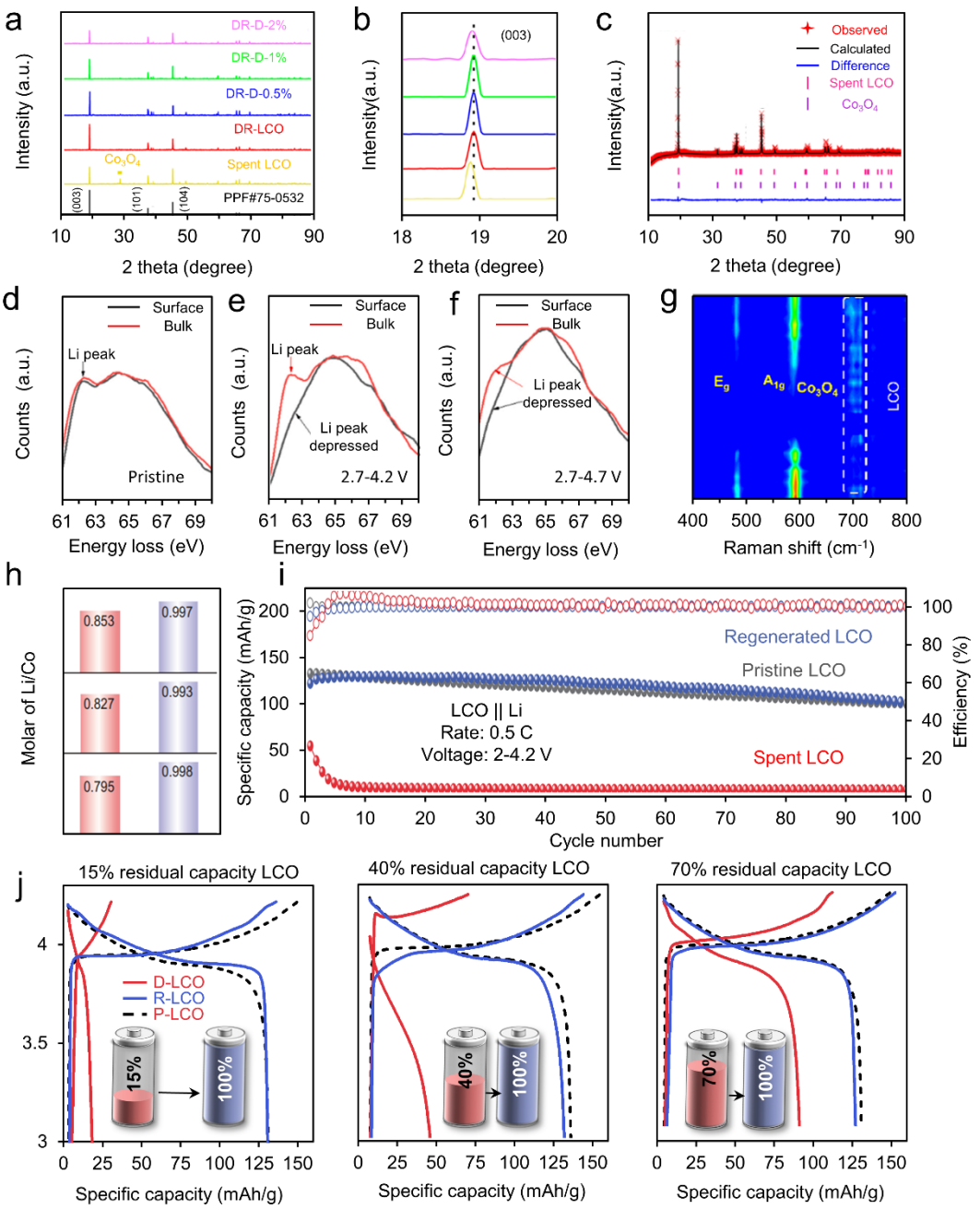

Figure 3. (a) The XRD patterns of spent LCO and regenerated LCO with different regenerated conditions. [55] Copyright 2021, American Chemical Society. (b) The enlargement of (003) peak for spent LCO and regenerated LCO with different regenerated conditions. [55] Copyright 2021, American Chemical Society. (c) The Rietveld refinements of spent LCO. [60] Copyright 2021, American Chemical Society. (d-f) EELS results of the pristine LCO, and the degraded samples at different cut-off voltages.[61] Copyright 2023, Elsevier. (g) The evolution of Raman patterns of LCO during cycling. [64] Copyright 2022, American Chemical Society. (h) The Li/Co molar ratio of spent LCO with different states of charge and the corresponding regenerated LCO. [65] Copyright 2022, Oxford University Press. (i) The electrochemical performance of spent LCO, regenerated LCO, and pristine LCO. [65] Copyright 2022, Oxford University Press. (j) Charge and discharge curves of spent LCO with different states of charge and regenerated LCO. [40] Copyright 2022, American Chemical

Society.

Zhang et al. demonstrated the Co_3O_4 phase formed on the surface (Figure 4a) of LCO during cycling at the atomic level by transmission electron microscopy (TEM), [66] which is confirmed by the XRD and Raman results. Li and Wang et al. found that there were obvious cracks and holes on the surface and inside (Figure 4b and Figure 4c) of the spent LCO[65,67], which formed due to stress concentration during cycling. The formation of Li vacancies in LCO is accompanied by vigorous Li^+ deintercalation and intercalation, causing uneven stress distribution in the LCO lattice structure, was proved by continuous changes of diffraction peak around 19° in the XRD pattern upon cycling. [68,69] AFM is often used to analyze the flatness of the material surface. Zhou et al. reported that the surface of the spent cathode materials showed obviously high fluctuations and roughness (Figure 4d-f) [40] due to the slippage of the LCO lattice structure in a specific direction during cycling. [70,71] They also observed the obvious cracks in the TOF-SIMS images of spent LCO. The areas near the crack have a concentrated distribution of Li/Co elements, [72] which was attributed to the defective structural part being more likely to react with the electrolyte. [71,73] Researchers have successfully evidenced the presence of a Co_3O_4 impurity phase on the surface of the depleted cathode material. Li vacancies contained in the spent cathode, and under the condition of low calcination temperature, some Li vacancies can be repaired, and then the disordered phase cannot be repaired (Figure 4g-i)[61].

In summary, according to the results of prior work, we have drawn the following conclusions. At the micron scale or sub-micron, the surface of spent LCO exhibits prominent cracks and voids, which can be analyzed through characterization techniques such as XRD, TOF-SIMS, AFM, and SEM. The occurrence of these cracks is intimately related to the continuous lattice expansion or contraction occurring during the cycling process of the LCO cathode material. At the nanoscale, the surface of spent cathode particles displays Co_3O_4 spinel structure (the emergence of the spinel phase is closely linked to the migration of transition metals into the lithium layers). Internally, there exists a lithium-deficient layered structure. The defective structure in spent LCO can be analyzed through techniques such as TEM and in situ Raman spectroscopy. We have

also found that effective restoration of the internally lithium-deficient layered structure can occur at temperatures as low as 300 ℃; however, the spinel structure formed on the surface requires a higher temperature for repair.

The mechanisms and methods for direct regeneration of spent LCO

The repair process of spent LCO is as follows:

$$Li_{1-x}CoO_2 + xLi^+ + xe^- \rightarrow LiCoO_2$$

$$Co_3O_4 + 6Li_2CO_3 + O_2 \rightarrow 12LiCoO_2 + CO_2$$

Researchers have directly repaired and regenerated spent LCO through solid-state sintering, electrochemical lithiation, solution lithiation, and lithiation assisted by deep eutectic solvents. For solid-state sintering, the spent LCO is mixed with a Li salt without destroying spent LCO, and the Li vacancies and Co_3O_4 that existed in spent LCO are repaired with calcination. [74,75] Yuan et al. directly combined spent LCO cathode materials with solid lithium compounds (such as Li_2CO_3 or LiOH) and annealed the mixture in the air at 850–950 °C for 12 h to repair the compositional and structural defects. [76] The physical, chemical, and electrochemical properties of the regenerated LCO are all close to those of commercial LCO, which fulfill the commercial requisites for reuse. During electrochemical lithiation, Li^+ in the solution is supplemented into the Li site of the spent cathode driven by an electric field. [77,78] He et al. used the spent LCO and Pt as the working and counter electrodes, respectively. The Li^+ in Li_2SO_4 electrolyte was delivered to the spent LCO during discharge, and the Li vacancy defects were repaired. [79] An electrode fabricated using the regenerated LCO materials displayed a charge capacity of 136 mAh/g, which is nearly equivalent to that of a commercial LCO electrode (140 mAh/g). Solution lithiation generally refers to the process of lithium supplementation for spent cathodes at high temperature and high pressure, where the sample can be further repaired after short sintering. [80] Chen and co-authors described a methodology involving the hydrothermal treatment of used cathode material particles within a specific concentration of lithium salt solution, succeeded by a brief thermal annealing step, to regenerate the cathode materials.[81] The rejuvenated LCO particles maintain their original morphology and structure, thereby delivering high specific capacity and robust cycling stability. Significantly, it was discovered that the

regenerated LCO exhibits a notably superior rate performance when compared to particles restored via solid state sintering methods. Deep eutectic solvents (DES) were also used to relithiate the spent cathode without high pressure. After re-lithiation, the spent LCO can be regenerated by solid-state sintering. Cheng et al. [65] obtained the regenerated cathode material by stirring spent LCO in LiCl–CH_4N_2O solvent at 120 °C and then calcining the treated sample at 850 ℃ for 2 hours (Figure 4j). The used deep eutectic solvents can repair the spent LCO with different states of charge. The rejuvenated LCO demonstrates a commendable capacity retention of 90% following 100 charge-discharge cycles, which parallels that of the original LCO. Notably, the DES utilized can be effortlessly recycled multiple times, rendering this method a notably eco-friendly option relative to conventional recycling procedures, given its non-generation of wastewater and minimal energy demands. The EverBatt 2020 assessment projects a potential financial gain of 1.7 US dollars/kg cell, underscoring the strong economic viability of this recycling process.

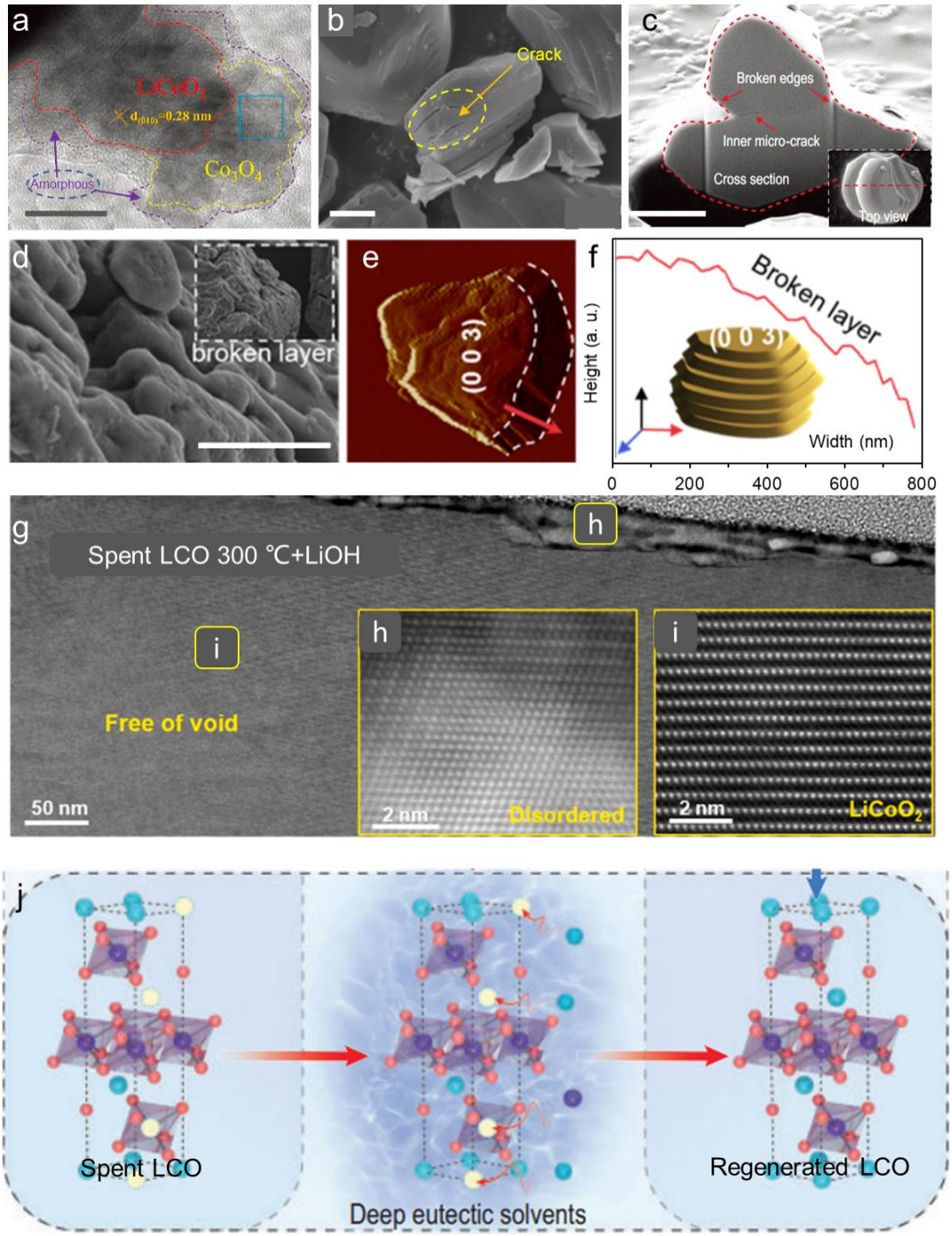

Figure 4. (a) TEM images of spent LCO (scale bar, 20 nm). [66] Copyright 2021, The Authors, published by MDPI. (b) SEM images of spent LCO (scale bar, 2 μm). Reproduced with permission.[67] Copyright 2020, American Chemical Society. (c) FIB-SEM images of spent LCO (scale bar, 2 μm). [65] Copyright 2022, Oxford University Press. (d-f) SEM and AFM images of spent LCO and corresponding results (scale bar, 1 μm). Reproduced with permission. [40] Copyright 2020, American Chemical Society. (g) TEM image showing the cycled sample annealed at 300 °C with LiOH (10 h). Void is successfully suppressed in (g). (h, i) Enlarged images showing the surface region "h" with disordered structure and the subsurface region "i" with well-defined layered structure.[61] Copyright 2023, Elsevier. (j) The schematic of direct regenerate spent LCO by deep eutectic solvents. [65] Copyright 2022, Oxford University Press.

Degradation mechanisms of $LiNi_xCo_yMn_zO_2$ (x+y+z=1) and corresponding characterization methods

Nickel–cobalt–manganese ternary cathodes have a lower cost than the LCO, and the ternary cathode with higher Ni content has higher energy density at the same cut-off voltage. However, high Ni content was reported to cause structural instability of the cathode during cycling. [82] Up to now, the ternary cathodes that have been commercialized include $LiNi_{0.3}Co_{0.3}Mn_{0.3}O_2$ (NCM111), $LiNi_{0.5}Co_{0.2}Mn_{0.3}O_2$ (NCM523), $LiNi_{0.6}Co_{0.2}Mn_{0.2}O_2$ (NCM622), $LiNi_{0.8}Co_{0.1}Mn_{0.1}O_2$ (NCM811) cathode materials. In the ternary cathode family, NCM523 has been extensively used in EVs due to its combined advantages in price and performance. [83] Hence, an increasing amount of spent NCM523 cathodes is anticipated to be scrapped shortly. In this section, we mainly summarize the structural defects and characterization methods of cycled NCM523.

Chen et al. [38] observed that spent NCM523, pristine NCM523, and regenerated NCM523 (R-NCM523, RA-NCM523) at different regenerated conditions keep a well-defined layered α-$NaFeO_2$ structure with R-3m space (Figure 5a). The diffraction peak near 19° corresponding to the (003) crystal plane and the diffraction peaks near 65° corresponding to the (110)/(108) crystal plane in spent NCM523 cathodes are significantly different from those of pristine NCM523. The diffraction peak corresponding to the (003) crystal plane in spent NCM523 distinctly shifts towards lower angles as compared to that of the pristine NCM523 sample (Figure 5b). This displacement is attributed to the occurrence of lithium vacancies within the spent NCM523, which consequently alters the lattice cell structural parameters inherent to the original NCM523 material. [84] The distinguished two peaks of the (110) and (108) plane were found to merge for the spent materials (Figure 5c), indicating that the inherent layered structure of pristine NCM523 has been destroyed and the rock salt/spinel phase has been formed after multiple charge-discharge cycles. [85] The Rietveld refinement results were used to quantitatively analyze the change of structural parameters and the degree of Li/Ni mixing. [86] The a lattice parameter decreased while the c parameters increased after cycling (Figure 5d). The Li/Ni mixing in the spent

NCM is 13.7%, which is greater than that of the pristine cathode (4.3%). The emergence of a defective structure (comprising rock salt and/or spinel phases) on the surface of heavily degraded NCM523 (referred to as HD-NCM523) results from the migration of transition metal elements to the lithium sites within the NCM523 crystal lattice during cycling (Figure 5e). TEM confirmed the structure and location of rock salts and spinel in the spent cathode.

Ma et al. determined the degradation degree of spent NCM523 cathode using ICP. They observed a direct correlation between the change in the elemental analysis and the measured discharge capacity of the spent positive electrode, [87] i.e., the lower the discharge capacity, the more degradation it suffered (Figure 5f). They also observed a rough surface of spent NCM523 with obvious microcracks and holes, which may be related to the side reactions with the electrolyte occurring on the surface during cycling. Obvious cracks and holes in spent NCM523 were further observed by FIB-SEM. The highly degraded $LiNi_{0.8}Co_{0.1}Mn0._1O_2$ (S-NCM) exhibits obvious cracks and holes at the surface and in bulk (Figure 5g). The bulk of repaired $LiNi_{0.8}Co_{0.1}Mn0._1O_2$ (S-NCM) showed a smooth surface (Figure 5h). Unlike NCM523, the repaired NCM still has a partial rock salt phase (Figure 5i-j)[88], which is closely related to the Li/Ni mixing caused by the large Ni content.[89] Similar to LCO, the lattice parameters of NCM523 and $LiNi_{0.8}Co_{0.1}Mn0._1O_2$ change during repeated charging and discharging,[51,69] and the stress caused by changes in lattice parameters after multiple cycles led to cracks in layered cathode materials. The structural evolution of the surface of NCM523 inevitably causes a change in the valence state of its surface elements during cycling. [90] Cheng et al. [87] observed that the Ni valence state of the spent cathode had changed significantly compared with that in pristine NCM523 using the XPS technique. The increased Ni^{2+} content is mainly due to the formation of NiO rock salt structure on the surface of NCM523 during the process of charging and discharging, which is further verified by the O1s peak results of the spent cathode. The transition metal Co valence state on the surface of spent NCM523 was found to be dominated by Co^{3+} without significant change. The Mn element on the surface of spent NCM523 presents a higher oxidation state relative to the regenerated cathode, which may be related to the charge

compensation of the Mn element by the formation of Li deficiency during cycling. Liu et al. discovered that the XPS spectra of the Co 2p3/2 and Mn 2p regions in the cathode material, both before regeneration (at a low SOH, denoted as L-NCM523) and after direct regeneration (at a high SOH, denoted as H-NCM523), exhibit nearly indistinguishable characteristic peaks corresponding to Co^{3+} and Mn^{4+} ions at binding energies of 780.2 eV, 642.3 eV, and 653.9 eV (Figure 5k-l). [91] The variation of Mn valence before and after the regeneration of cathode materials is inconsistent with the above literature reports, which may be related to the degree of failure of the material. Direct regeneration led to a significant increase in Ni (III) content in NCM523 (Figure 5m), confirming the transformation of the impurity phase to a perfect layered structure. Significantly, the cathode materials regenerated through the novel process showcased appreciably enhanced capacities, outperforming those attained via conventional and exclusive eutectic salt-based regeneration techniques, and indeed, they marginally exceeded the performance of commercial NCM materials. The organic molten salt system used in the process of regenerated creates an oxidative environment during the repair process of the failed NCM, thereby realizing the transformation of Ni from a low valence state to a high one. This effectively reduces Li/Ni mixing in the regenerated cathode material, resulting in regenerated NCM exhibiting better electrochemical performance compared to pristine cathode materials. Taking into account the economic and environmental advantages offered by the organolithium salt-assisted eutectic salts direct regeneration method, it reveals potential for the direct restoration of low SOH NCM cathodes and displays competitiveness suitable for industrial-scale applications.

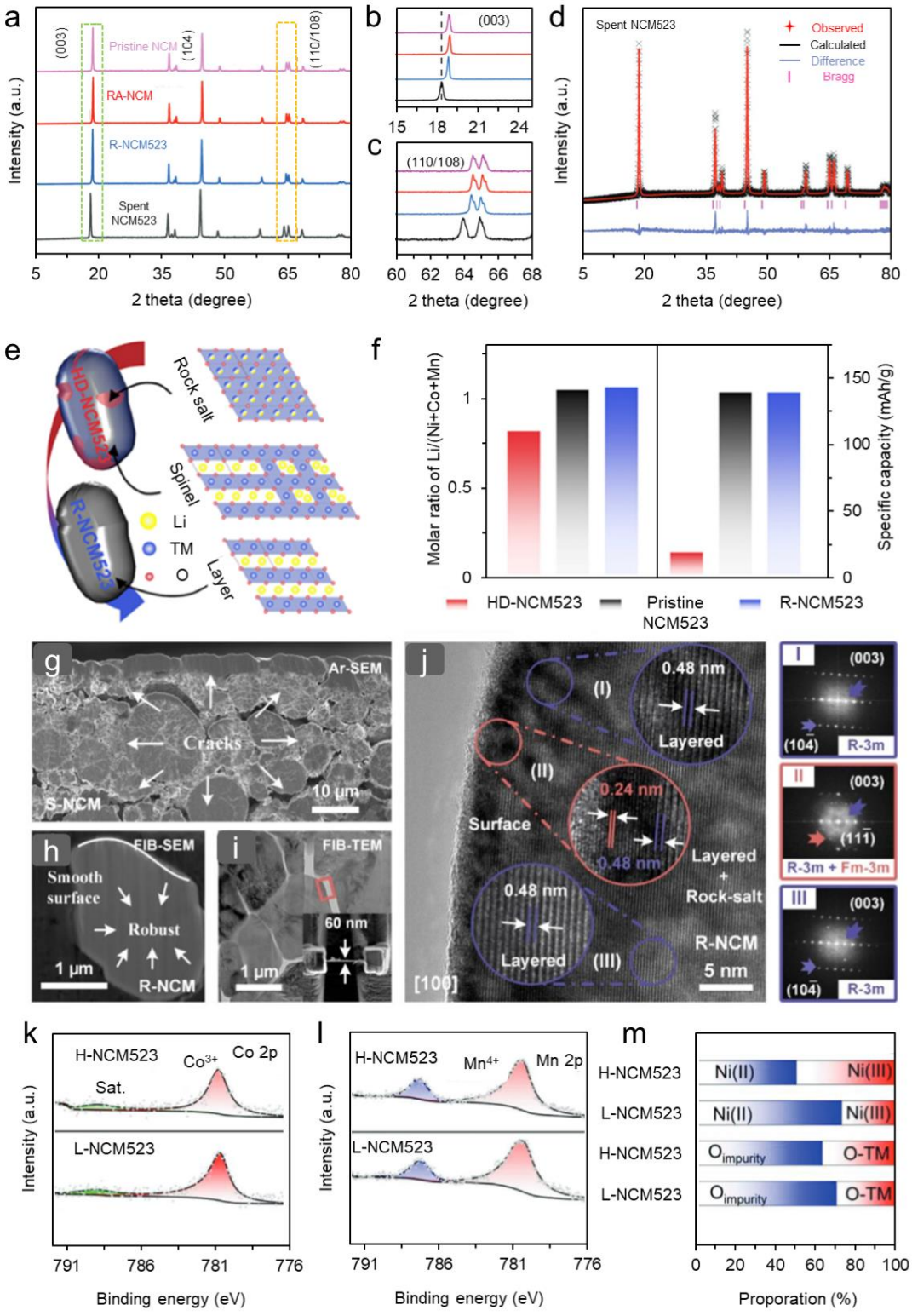

Figure 5. The XRD patterns of spent NCM523, pristine NCM523 and R-NCM523, RA-NCM523.[38] Copyright 2022, WILEY-VCH Verlag GmbH & Co. (a) (5-80°). (b) (15-24°). (c) (60-68°). (d) Rietveld refinements of spent NCM523. [38] Copyright 2022, WILEY-VCH Verlag GmbH & Co. (e) Schematic of the rock salt, spinel of HD-NCM523, and layer structure of R-NCM523. [87] Copyright 2022, American Chemical Society. (f) The molar ratio of Li/(Ni+Co+Mn) of HD-NCM523, pristine NCM523 and R-NCM523. [87] Copyright 2022, American Chemical Society. (g) Cross-section SEM

image of S-NCM prepared by Argon ions polishing. (h) Cross-section SEM image of R-NCM obtained by FIB. (i) FIB-TEM samples of R-NCM. (j) HRTEM image of R-NCM, and the FFT images on the right correspond the circle areas in R-NCM.[88] Copyright 2023, WILEY-VCH Verlag GmbH & Co. (k-l) XPS spectra of Co 2p, and Mn 2p in L-NCM523, and H-NCM523. (m) The proportion changes of O and Ni contents in L-NCM523, and H-NCM523. [91]Copyright 2023, WILEY-VCH Verlag GmbH & Co.

Cheng and co-authors [50] identified the presence of cracks on the surfaces of the degraded NCM523 cathode. (Figure 6a). TEM was used to analyze the structural characteristics of spent cathode materials. The TEM images of spent NCM523 (Figure 6b and Figure 6c) showed that the spent cathodes exhibit different lattice structural characteristics from the surface to the bulk. The HRTEM images of the outermost surface of spent NCM523 showed that the lattice-fringe spacing of its structure is 0.24 nm (Figure 6d), indicating the outermost surface of spent NCM523 is composed of rock salt phase (NiO). This agrees with previous works and was confirmed by the fast Fourier transform (FFT) pattern (Figure 6d). [38,85] The formed rock salt phase was attributed to the transition metals located in the transition metal layer migrating to the Li layer. [92] It was also found that the lattice fringe spacing increased to 0.51 nm for the area close to the internal region of the spent material (Figure 6e and Figure 6f), which is slightly larger than the lattice fringe spacing (0.48 nm) of the pristine NCM523 cathode (003) crystal plane. [93] The increased lattice fringe spacing was attributed to the migration of elements located in the transition metal layer to the Li layer during cycling, whose formation mechanism is similar to that of the rock salt phase. [94] Qin et al. [38] found that the innermost structure of the spent cathodes is still completely layered but lacking Li. Chen et al. [95] conducted a detailed analysis of the coordination of O elements and the oxidation state of transition metals at different regions (surface and bulk) of spent NCM523 cathode through EELS. The peak observed in the O K-edge spectrum at 534 eV represents the transition of O 1s electrons to hybridized states, which involve a combination of TM 4sp and oxygen 2p orbitals. The features in the pre-edge region situated below 534 eV correspond to transitions to energy states constituted by TM 3d and oxygen 2p orbitals. The disappearance of the O element pre-edge structure at the surface relative to the bulk phase of spent NCM523 was referred to the change in the coordination structure for the O element and the transition metal element (Figure 6g)

due to the rock salt/spinel phase formation on the surface of cathode materials during cycling. For the O K-edge spectra (bulk) of cathode materials, the spectra of the spent cathodes are consistent with that of the regenerated cathode (Figure 6g), indicating no obvious structural change in the bulk of the spent cathode materials. For the Mn L-edge spectra of spent NCM523, the Mn L-edge spectra of the surface were observed to have redshifted relative to the bulk, suggesting that the Mn in the surface region is in a low oxidation state, which may be related to the charge compensation caused by the release of lattice oxygen during the charging and discharging process of the cathode materials. [96] The Mn L-edge spectra of the regenerated cathode (including the bulk and surface) are consistent with the bulk of the spent cathode (Figure 6h), indicating the valence state change of the Mn element only occurs on the surface of the NCM523 cathode material. The Co L-edge spectra (including the bulk and surface) of the spent and the regenerated cathodes are almost identical (Figure 6i), which was believed to be Ni is the main valence element in ternary cathode materials during cycling, and the proportion of Co redox is much smaller than Ni redox. In Ni L-edge spectra (Figure 6j), the Ni element of the regenerated NCM523 (including the bulk and surface) exhibits a lower oxidation state compared to spent NCM523 (including the bulk and surface), this phenomenon was attributed to the charge compensation resulting from the reintroduction of lithium following the regeneration process. After investigating the literature, we found that the oxidation state of Ni elements and Mn elements on the surface of the spent NCM523 cathodes and regenerated NCM523 cathodes is indeterminate, [38,87,95-98] which may be related to the failure state and repair degree of the cathode material. In general, the lattice structure of ternary cathode materials still maintains the original inherent layered structure after cycling, and Li vacancies will appear inside the particles, which is the main factor for its lack of capacity and rock salt/spinel phase formation on the surface of spent cathode particle. [50,87,96] The formed rock salt/spinel phase is due to transition metals migrating to the Li site (Figure 6k), and this structure is not conducive to Li^+ transport, which is the primary cause of the inadequate cyclic stability in cathode materials.

The mechanisms and methods for direct regenerate spent $LiNi_xCo_yMn_zO_2$

(x+y+z=1)

There are internally existing Li vacancies and surface-formed rock salt/spine phase defects for the spent ternary cathodes. Researchers have directly repaired and regenerated the spent ternary cathode using different methods (solid-state sintering, solution-based lithiation, molten salt-based lithiation, and ionic liquid-based relithiation), and the repaired cathode materials demonstrate a capacity that is commensurate with their pristine counterparts. The regeneration process of spent ternary cathodes is similar to that of LCO, which transforms the rock salt/spinel phase that resides on the surface of degraded cathodes into a perfect layered structure, and the Li vacancies existing in the internal structure disappear by re-lithiation during the regenerating process. The following equations can summarize the reaction that occurs during the repair process, where Me represents the transition metal elements (Ni, Co).

$$Li_{1-x}MeO_2 + xLi^+ + xe^- \rightarrow LiMeO_2$$

$$Me_3O_4 + 6Li_2CO_3 + O_2 \rightarrow 12LiMeO_2 + CO_2$$

$$MeO + 0.5Li_2CO_3 + 0.25O_2 \rightarrow LiMeO_2 + 0.5CO_2$$

Traditional solid-state sintering techniques can efficiently revitalize layered ternary cathode materials. [97,99-102] Sun et al. [103] achieved a good degree of repair and regeneration of spent NCM111 with an extra mechanochemical step before the solid-state sintering. Their innovative hybrid process successfully reinstated the layered structure and augmented Li^+ diffusion, without incorporating additional impurities. Upon regeneration, the NCM materials exhibited an initial discharge capacity of 165 mAh/g at a 0.2C during the first cycle, and maintained a capacity retention of over 80% even after 100 cycles. Cao et al. [100] developed a simple and efficient non-destructive method to recover cycled NCM523 particles from spent LIBs by heat treatment, which can fully restore the capacity and the cycle stability of NCM523 compared to pristine cathodes. The regenerated materials showcased a discharge capacity of 162.0 mAh/g at a 0.1C. Under 1 C cycling condition, the materials delivered an impressively reversible discharge capacity of 128.6 mAh/g after 100 cycles, retaining 91.9% of their initial capacity, thus demonstrating parity with the pristine NCM523 in terms of capacity retention. Zhang et al. [102] reported a simple and greener regenerative approach by pre-

oxidizing the spent NCM622 before short annealing approach. The rejuvenated cathode material has a well-preserved crystalline structure and a notably diminished Li/Ni intermixing, manifesting a capacity of 153.82 mAh/g (1C) at the voltage window of 2.8 to 4.3 V, with a remarkable capacity retention of up to 94.74% following 100 cycles. Cheng's group turns the rock salts/spinel phase presented on the surface of the spent cathode into transition metal hydroxides by hydrothermal treatment of spent NCM523. The materials obtained after hydrothermal treatment was mixed with LiOH and calcined. The defects of the spent cathode materials were directly repaired by topotactic transformation. [50] Interestingly, the topotactic lithiation process featuring notably low migration barriers was linked to facile movement of Li^+ within a channel (reduced electrostatic repulsion), where ions migrate from one octahedral site to another, traversing a tetrahedral intermediate. This unique characteristic significantly bolstered the efficiency of lithium replenishment during the regeneration. The solution relithiation is a relatively simple and scalable technology for regenerating the LIB cathodes,[96,104]-despite the need for high pressure. The spent cathodes can be restored to a reasonable degree after solution re-lithiation and mild annealing. Chen et al. [105] implemented a recycling strategy for severely deteriorated NCM523 cathode materials (with residual capacity approximating 10%) by employing a two-step process that integrated hydrothermal treatment with a solid-state eutectic Li^+ molten-salt solution sintering procedure. The regenerated cathodes exhibited a layered crystalline structure, and the capacity of pouch cells (1.7 Ah) assembled by regenerated cathodes maintained 90.8% after 500 cycles. Another potential regeneration solution for spent cathodes is a molten salt (eutectic mixture). [38,95,97,108] Zhou group [87] opted for a eutectic LiI-LiOH salt system, characterized by the lowest eutectic temperature among binary lithium salt eutectics, to create a Li-enriched molten environment conducive to the direct regeneration of various spent ternary cathode materials, including NCM111, NCM523, and NCM622. Ionic liquids are also considered effective media for solution repair because, like molten salts, they do not require extreme high-pressure conditions. The capacity, rate capability, and cycling performance of the regenerated NCM523 were comparable to that of the pristineNCM523. After 200 cycles, the capacity retention

exceeded 80%, and following 300 cycles, it maintained at 73%. In Dai's recent work, [45] ionic liquids were employed as the fluxing solvent, utilizing LiBr as the lithium source, to regenerate the delithiated NCM111 material through an ionothermal treatment process, subsequently followed by calcination at a temperature of 500 ℃ for a duration of 4 hours. For the first cycle, the charge capacity of regenerated NCM523 was recorded to be 173.6 mAh/g at 0.1C, comparable to that of commercial NCM523 (175.3 mAh/g) and much larger than that of spent NCM523 (145.9 mAh/g). Chen and colleagues transformed discarded polycrystalline $LiNi_{0.88}Co_{0.095}Al_{0.025}O_2$ (S-NCA) into high-value single-crystal cathode materials by employing a straightforward yet practical LiOH-Na_2SO_4 eutectic molten salt approach. (Figure 6l). The discharge and charge capacity of regenerated $LiNi_{0.88}Co_{0.095}Al_{0.025}O_2$ (R-NCA) were recorded to be 204.8 and 226.0 mAh/g at 0.1C, respectively. Following 250 cycles at 1C, the regenerated R-NCA managed to sustain a discharge capacity of 160.1 mAh/g, representing 85.1% of its initial capacity. The variation in Ni chemical state and energy band configurations within NCA that occurred during the regeneration process is depicted in Figure 6m. [51] We believe that this methodology stands to be effectively adapted and applied to a range of alternative cathode materials, such as $LiNi_xCo_yMn_zO_2$ (NCM) and spent NCA experiencing differing levels of lithium depletion.

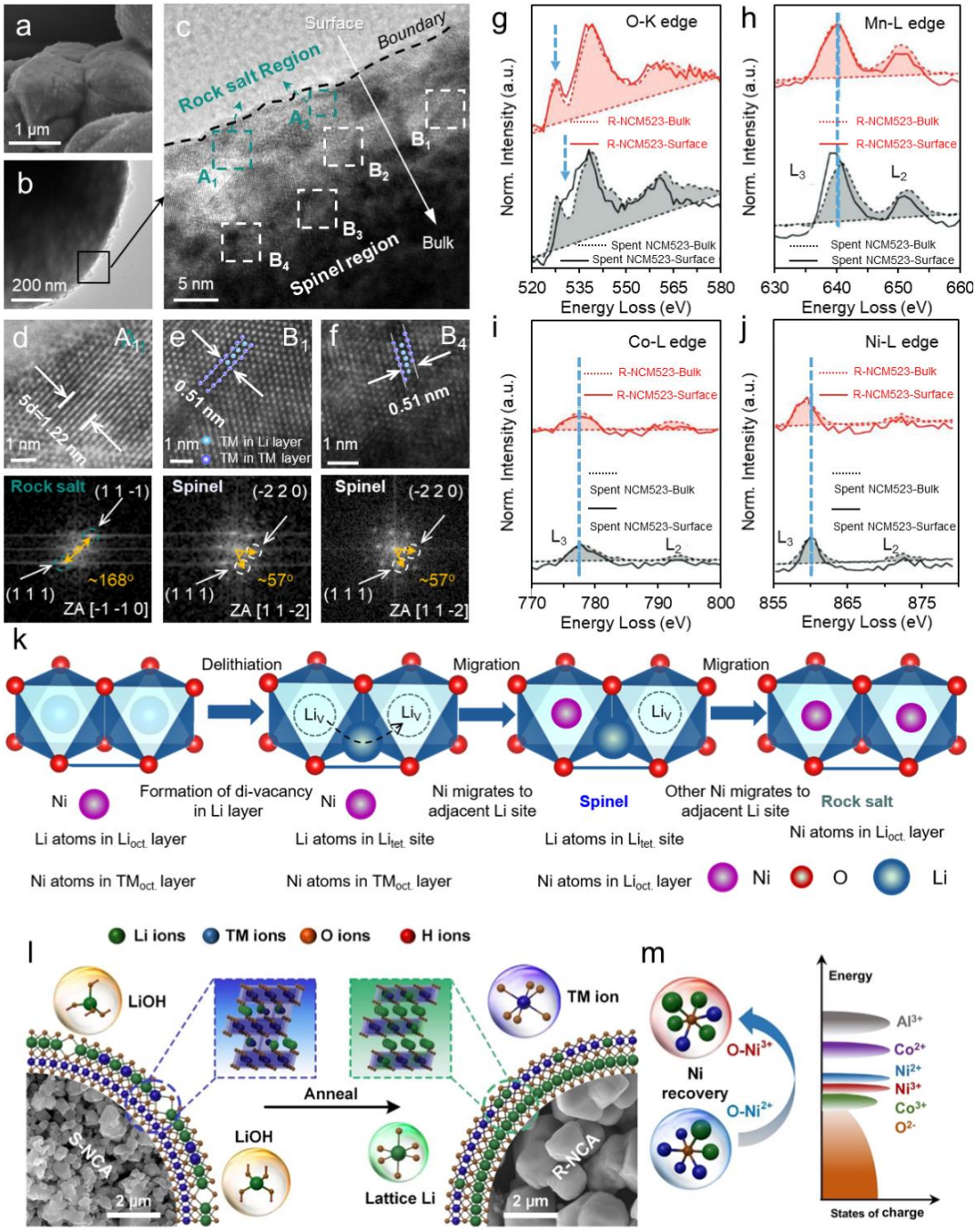

Figure 6. (a, b) SEM and TEM image of spent NCM523. [50] Copyright 2023, American Chemical Society. (c) The HRTEM images of spent NCM523. Copyright 2023, American Chemical Society. (d-f) HRTEM images and the corresponding FFT patterns of the dashed boxes (A1, B1, B4) in (c).[50] Copyright 2023, American Chemical Society. (g-j) EELS spectra of O-K edge, Mn-L edge, Co-L edge, and Ni-L edge of spent NCM523 (spent NCM523-bulk, spent NCM523-surface) and R-NCM523 (R-NCM523-bulk, R-NCM523-surface). [95] Copyright 2019, WILEY-VCH Verlag GmbH & Co. (k) Schematic of degradation mechanisms of NCM523 cathode materials. [50] Copyright 2023, American Chemical Society. (l) The evolution of surface structure during the treatment. (m) The change of Ni chemical state during regeneration and the energy band structures in cathode materials. [51]Copyright 2023, WILEY-VCH Verlag GmbH & Co.

Degradation mechanisms of $LiFePO_4$ and corresponding characterization

methods

$LiFePO_4$ (LFP) has attracted widespread attention due to its low cost and stable long-cycle performance, with a clearly growing market. [109-111] For the spent LFP, the researchers demonstrated that Li vacancies are the main reason for the capacity loss. [2,6,39,49,112,113] Ji et al. [2] measured the concentration of the Li vacancies using ICP. They found that the Li/P (0.92) and Li/Fe (0.98) molar ratio in spent LFP (S-LFP) are lower than the Li/P (1.07) and Li/Fe (1.07) molar ratio (Figure 7a) in pristine LFP (P-LFP). As a result, LFP will form $FePO_4$ due to the presence of Li vacancies, as confirmed by the XPS spectra of S-LFP, which shows a distinct characteristic peak of Fe^{3+} belonging to $FePO_4$, while regenerated LFP (R-LFP) has almost no characteristic peaks of Fe^{3+} (Figure 7b). XRD is often used to detect the impurity phase of spent cathode materials. They also observed that the phase structure of S-LFP also maintains the inherent olivine structure with the Pnma space group of pristine LFP, but the XRD patterns of S-LFP also showed a significant diffraction peak of $FePO_4$ (Figure 7c), which is attributed to the presence of Li vacancies in spent LFP. Cheng et al.[52] found that the appearance of Li vacancies not only produces the $FePO_4$ phase but also causes Li/Fe antisite defects in S-LFP, which is caused by the migration of Fe atoms to the Li site in LFP. [49] XRD Rietveld refinement is used to analyze the concentration of Li/Fe antisite defects in S-LFP (Figure 7d), and it turned out to be 4.28%. The formation of Li/Fe antisite defects will hinder Li^+ transport during the charging and discharging process, which is the reason for the poor cycle stability of LFP after repeated cycles.[49,52,114-116] FTIR spectroscopy is also a frequently used method for characterizing Li/Fe antisite defect. [117,118] The concentration of antisite defect in LFP is related to the peak position around 1000 cm^{-1} in the FTIR pattern, and higher wavenumbers mean higher concentrations of antisite defects in LFP. [119] The position of antisite defects characteristic peak of S-LFP offset to the right relative to R-LFP, indicating that its Li/Fe antisite defects concentration is increasing during cycling (Figure 7e). Operando neutron diffraction was utilized to precisely measure and track the development of Li/Fe antisite defects over time. Chen's group [49] observed the evolution of antisite defects concentration of LFP cathode 3by in site neutron diffraction during regenerating (Figure 7f). After

regeneration, the concentration of the Li/Fe antisite defects of LFP decreased significantly. EELS is an effective method for obtaining physical and chemical information about the surface of materials. Cheng's group [2] analyzes the atomic chemical state at different regions on the surface of the S-LFP particle by EELS. The O-K edge spectra at different positions of the S-LFP cathode particles showed obvious differences. The O-K edge spectra obtained by the partially selected positions of the spent cathode surface have pre-edge, but that of the other positions does not show any. Here, the presence or absence of pre-edge in the O-K edge spectral line represents a change in the coordination environment of O, [95] indicating the phase structure of different regions on the surface of S-LFP is disparate. It is generally believed that the presence of pre-edge in the O-K edge line of S-LFP indicates the presence of Fe^{3+} ($FePO_4$), [2,120,121] which is confirmed by the higher oxidation state of Fe in the Fe-L edge line. The ELLS characterization of the spent LFP was also performed by Chen group, [49]and the results showed that there were different phase structure ($FePO_4$ and $LiFePO_4$) distributions on the surface and inside the spent LFP (Figure 7g). For the O-K edge line, some regions of S-LFP do not show the pre-edge, indicating that the structure of this region is still LFP. The analysis of EELS spectra at the O-K edge and Fe-L edge regions from the used cathode reveals evidence for the coexistence of LFP and $FePO_4$ phases on the surface of the S-LFP material. The results of O-K edge and Fe-L edge spectral lines (Figure 7i) at different selected regions on the surface of the regenerated LFP particles prove the uniformity of the surface structure of the regenerated cathodes, and its phase structure is LFP.[49] The lattice structures corresponding to $FePO_4$ and $LiFePO_4$ are shown in Figure 7h and Figure 7j. [122] It is worth noting that they found that the surface of the failed LFP is $LiFePO_4$ phase and the interior is $FePO_4$ phase. We have also investigated the microstructure of failed LFP, which have a surface structure of $FePO_4$ phase and an internal structure of $LiFePO_4$ phase. In degraded layered cathode materials, the surface generally is defect structure (spinel and rock salt) and the interior is layered structure with Li deficient, which is different from the distribution of defect structures of degraded LFP. The occurrence of different phase distributions on the surface and in the bulk of degraded LFP may be related to the non solid solution

reactions that occur during the electrochemical process.

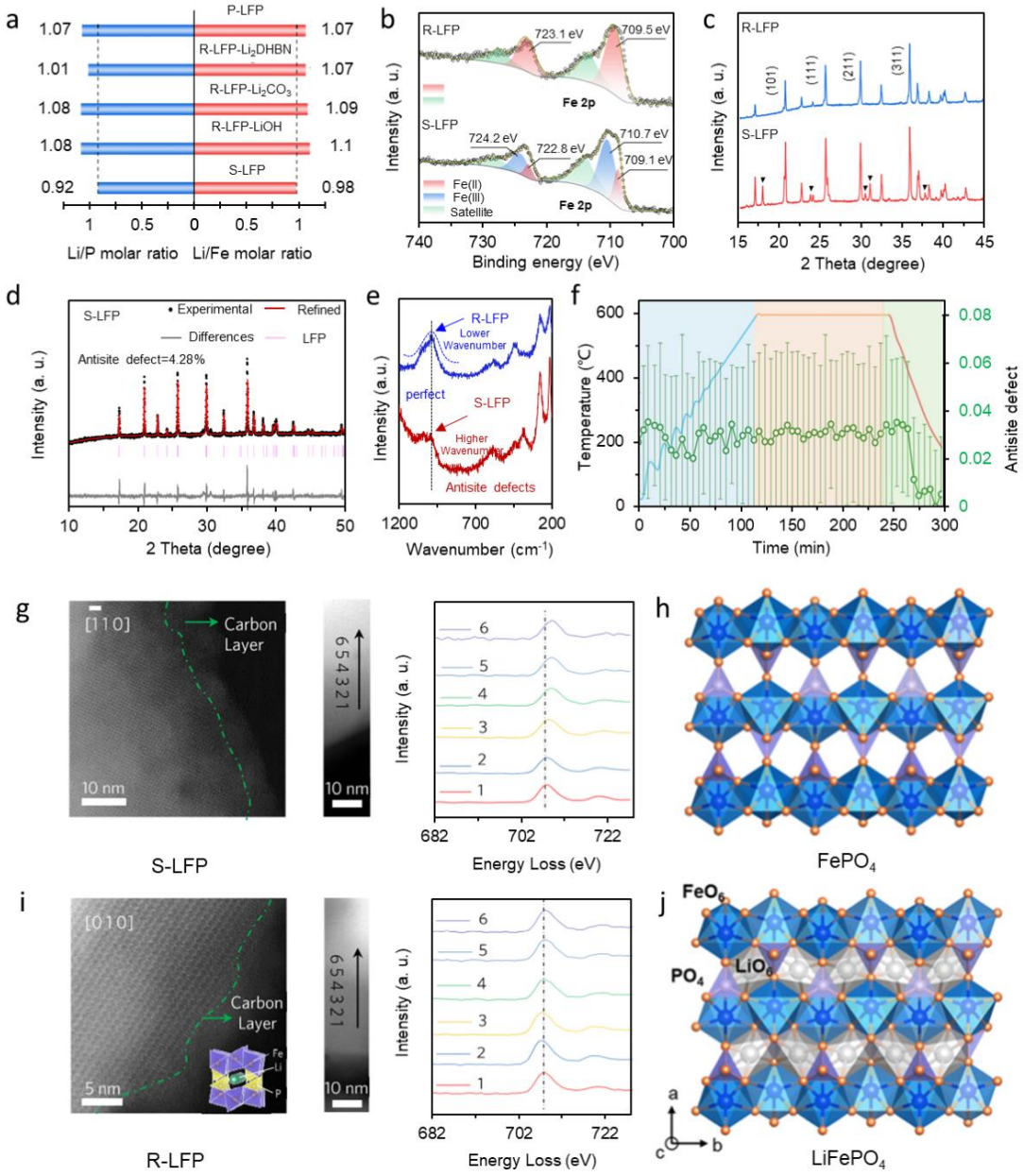

Figure 7. (a) The ICP results of S-LFP, P-LFP, and regenerated LFP (R-LFP-Li_2DHBN, R-LFP-Li_2CO_3, R-LFP-LiOH) by different methods. [2] Copyright 2023, Springer Nature Limited. (b, c) XPS and XRD results of S-LFP and R-LFP. Copyright 2023, Springer Nature Limited. (d) Rietveld refinement of S-LFP. [2] Copyright 2023, WILEY-VCH Verlag GmbH & Co. (e) FTIR spectra of S-LFP and R-LFP. [52] Copyright 2023, WILEY-VCH Verlag GmbH & Co. (f) The evolution of antisite defects upon heating (blue line), holding (orange line), and cooling (red line). [49] Copyright 2020, Elsevier Inc. (g, i) EELS (Fe-L-edge) of S-LFP and R-LFP. [49]Copyright 2020, Elsevier. (h, j) The lattice structure of $FePO_4$ and $LiFePO_4$.[122] Copyright 2023, American Chemical Society.

Cheng et al. [52] observed the surface morphology and defective structure of S-LFP by SEM and TEM. The SEM images present that the surface of S-LFP is flat and smooth (Figure 8a), which is different from the surface of spent LCO and NCM ternary cathode

materials with cracks. The TEM and HRTEM images of the spent LFP showed a carbon layer wrapping the LFP particles (Figure 8b and Figure 8c), and the particles have unsharp lattice structure from the surface to bulk (Figure 8c). They observed $FePO_4$ phase on the outer surface while the pristine LFP phase dominates the interior region. The boundary region of the two phases is the disordered structure phase (Figure $8c_1$-$7c_3$). However, the R-LFP surface did not vary significantly (Figure 8d) compared to the S-LFP cathodes. The R-LFP cathode showed obvious lattice structural periodicity from the surface to the bulk (Figure 8e and Figure 8f), and the entire regions of the particle are composed of the LFP phase (Figure $8f_1$-$7f_3$). The results of XPS depth profiles showed apparent Fe(III) characteristic peaks on the surface of the S-LFP particles, which corresponded to the existing $FePO_4$ phase.[2] As the etching depth increased, the position of the characteristic Fe peak shifted towards lower binding energy, signifying that the Fe valence state within the S-LFP transformed to Fe(II). This change corresponds to the presence of the LFP phase. The XPS and high-resolution TEM (Figure 8c) results confirmed that the surface of S-LFP comprises $FePO_4$, and the bulk of S-LFP is still LFP phase. Yuichi Ikuhara et al.[123] found that the phase structure ($FePO_4$ and LFP) distribution of delithiated LFP is uneven in the nm size range (Figure 8g-j), and the non-uniform reaction of electrode materials during the cycle would increase the Li^+ migration barrier, which may be the fundamental reason for the failure of LFP electrode materials. In addition, Cheng et al. [2] also found that the carbon layer on the surface of the LFP particles was damaged after multiple cycles, which is detrimental to the cycling and rate performance of LFP. [124-126] The R-LFP produced by the designed organolithium salt method presents a uniform carbon layer structure. Based on the current research, it is found that the surface morphology of LFP is maintained after multiple cycles, with a small partial lattice structural change [39,127] The main defects of cycled LFP are Li vacancies and Li/Fe antisite defects. [49,52,127-131] The formation of Li vacancies generates the $FePO_4$ phase, and the formed $FePO_4$ is mainly on the surface of S-LFP particles, while the bulk of the S-LFP particles is still in the LFP phase. Damaging the protective carbon layer after long-term cycling is also a defect of S-LFP. [2] Besides the main olivine LFP and $FePO_4$ phases found in spent LFP,

Li_3PO_4, P_2O_5, and Fe_2O_3 minor impurities were also observed in the cycled LFP. [132] The appearance of different defective structures may be closely related to the degree of degradation of S-LFP.

The mechanisms and methods for direct regeneration of spent LFP

The following formula can describe the repair process for a failed LFP:

$$Li_{1-x}FePO_4 + xe^- \rightarrow LiFePO_4$$

The most explored methods for repairing defects of S-LFP are solid-state sintering, electrochemical lithiation, solution lithiation, and molten salt lithiation. In the process of solid-state regeneration for S-LFP, the core mechanism involves restoring the Li^+ that were lost from the cathode during charge-discharge cycles by applying heat to spent cathode materials in combination with a lithium-rich compound.[132-136] Cheng et al. [2] mixed the highly reducing multifunctional organic lithium salt with spent LFP and calcined mixture to realize effective regeneration. In the direct regeneration process, organic lithium salts with reducing ability and sufficient Li^+ were used to repair the Li vacancies and antisite defects of S-LFP. In addition, the uniform carbon layer formed by the decomposition of organic lithium salts during calcination can restore the broken carbon layer of S-LFP. The restored LFP cathode shows good cycling stability and rate performance (high-capacity retention of 88% after 400 cycles at 5 C). Electrochemical relithiation is a less energy-intensive tactic to repair LFP. [6,113,137] Guo et al. [6] proposed a method for direct regeneration of S-LFP via an in situ charging and discharging process with a functionalized pre-lithiation separator (Figure 8k). This repaired method greatly reduces the cost of regenerating spent cathodes without damaging the structure of the cathode. Solution relithiation is a common method to regenerate spent LFP. [39,49,138] Jia et al.[52] repaired the S-LFP by hydrothermal treatment and subsequent calcination, with ethanol as a reducing agent and lithium acetate as a lithium. In addition, a heterogeneous interface containing N is constructed during regeneration, and the d-band center of Fe is regulated by the heterogeneous interface, which inhibits the generation of Li/Fe antisite defects of R-LFP during cycling. The suppression of the antisite defects during cycling significantly increased the cycle life of the regenerated cathode.

An eutectic molten salt can work simultaneously as a source of lithium and a solvent for the parasitic phases. Xia et al. [128] used $LiNO_3$:FeC_2O_4 as molten salt and mixed them with the spent LFP with a ratio of 0.5:0.1:1 and heated at 300 °C to allow the salt to melt—the complete regeneration of the S-LFP required a further annealing step at 650 °C to recover the LFP particles. The rejuvenated LFP displayed a discharge capacity of 145 mAh/g when tested at a rate of 0.5C, demonstrating an improvement exceeding 10% over the initial S-LFP capacity. Guo and colleagues [109] put forth a holistic approach to LFP recycling, which entails the direct regeneration of the deteriorated LFP materials using lithium compounds extracted from exhausted anodes. Moreover, inter-particle three-dimensional (3D) conductive networks are re-built via an in-situ carbonization of the polyvinylidene fluoride (PVDF) present between the particles of the spent LFP cathodes, enhancing the electrical conductivity and improving cycling performance of the regenerated LFP. Consequently, a better electrochemical performance was achieved in the regenerated LFP materials comparable to that of pristine LFP (Figure 8l).

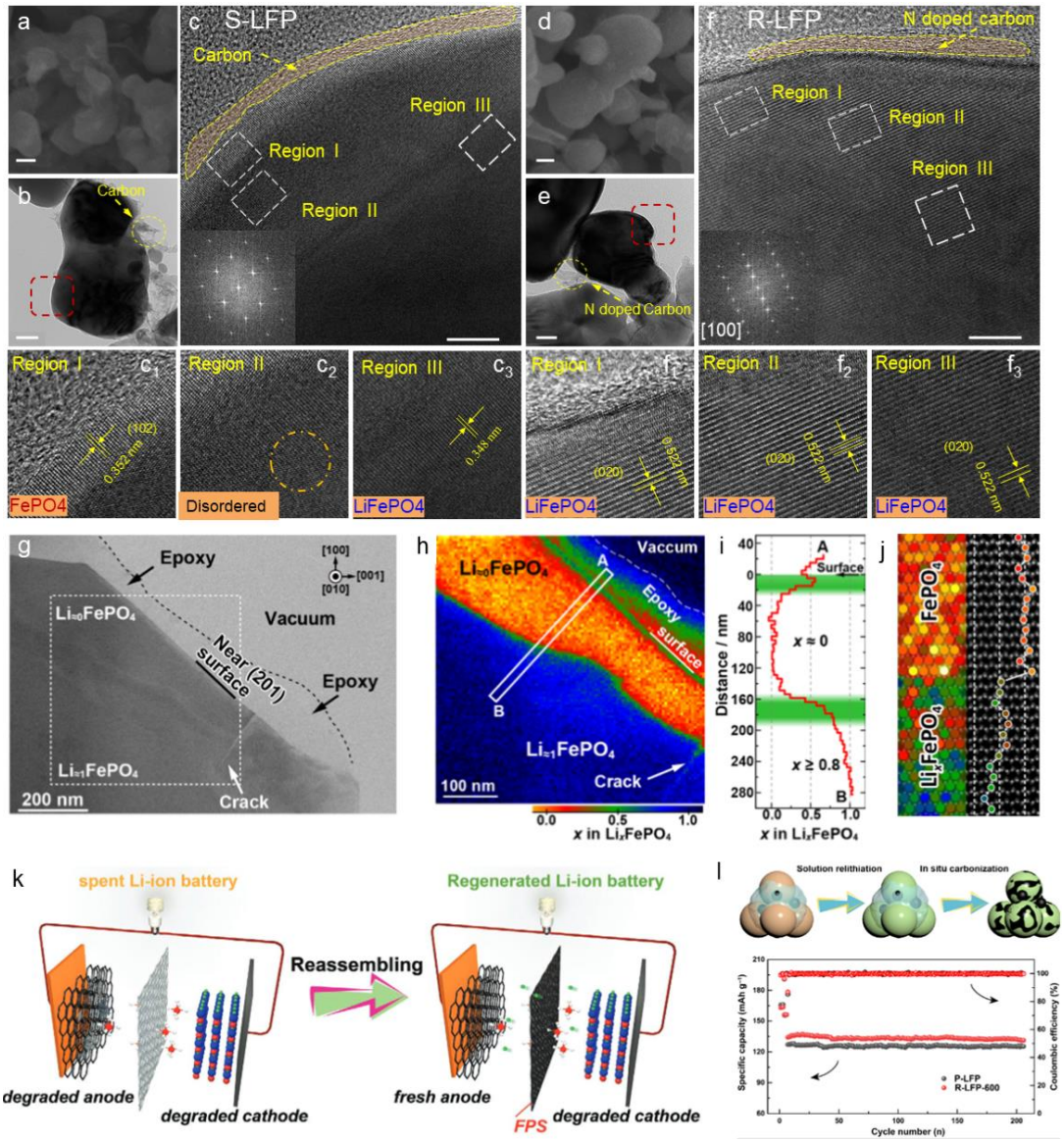

Figure 8. (a, b) SEM, TEM images of S-LFP. Scale bar, 100 nm. [52] Copyright 2023, WILEY-VCH Verlag GmbH & Co. (c) HRTEM images of S-LFP. Scale bar, 10 nm. (c_1-c_3) The enlargement of region I-III in Figure 8c. [52] Copyright 2023, WILEY-VCH Verlag GmbH & Co. (d) SEM images of R-LFP. [52] Scale bar, 100 nm. Copyright 2023, WILEY-VCH Verlag GmbH & Co. (e) TEM images of R-LFP. [52] Scale bar, 50 nm. Copyright 2023, WILEY-VCH Verlag GmbH & Co. (f) HRTEM images of R-LFP. (f_1-f_3) The enlargement of region I-III in Figure 8f. [52] Copyright 2023, WILEY-VCH Verlag GmbH & Co. (g) Low-magnification TEM image of an $LiFePO_4$ single crystal after chemical delithiation. (h) Li concentration map of delithiated $LiFePO_4$ from (g). (i) concentration profile between points A and B in (h). (j) Color map of columnar Li contents at different region in delithiated $LiFePO_4$, estimated using the quantitative EELS analysis result.[123] Copyright 2020, American Chemical Society. (k) Schematic illustration of the direct regeneration strategy based on functionalized prelithiation separator.[6] Copyright 2022, WILEY-VCH Verlag GmbH & Co. (l) Schematic illustration of the in situ carbonization process during the regeneration of spent LFP and the electrochemical performance of regenerated.[109] Copyright 2023, Chinese Chemical Society.

Degradation mechanisms of LMO and the corresponding characterization

methods

With the aim to develop affordable LIB technologies, LMO cathode materials are witnessing a growing prevalence in electric vehicles (EVs) and large-scale energy storage applications. [139,140] The degraded LMO cathode materials, similar to other spent cathodes (LCO, LFP, $LiNi_xCo_yMn_zO_2$ (x+y+z=1)), contain Li vacancies, which is the reason for the low capacity of the spent LMO. [141-143] Qian et al. [142] selected five samples with different degradation degrees (LMO (P-LMO), $Li_{0.822}Mn_2O_4$ (S-LMO-1), $Li_{0.665}Mn_2O_4$ (S-LMO-2), $Li_{0.592}Mn_2O_4$ (S-LMO-3) and $Li_{0.2}Mn_2O_4$ (S-LMO-4)) and studied their chemical and physical performance. The XRD peaks of these samples with different degrees of failure shifted significantly to the right relative to P-LMO (Figure 9a), indicating that the generation of Li vacancies will cause the LMO lattice to shrink, and the higher Li vacancy concentration, the more severe contraction of the lattice structure. They further tested the electrochemical performance of those samples, and the results showed that P-LMO delivered the highest 129.7 mAh/g charging capacity, and D-LMO-4 presented the lowest discharge capacity of 9.6 mAh/g, suggesting the Li vacancy concentration of the degraded LMO is closely related to its charging capacity (Figure 9b). The ICP results of these samples also demonstrate that Li vacancies are the dominant defect type in the spent cathode (Figure 9c). Typically, at the end-of-life stage, a battery exhibits a capacity decrease of about 20%, which generally results from the synergistic effects of losing lithium content. Consequently, they chose the chemically desodiated $Li_{0.822}Mn_2O_4$ cathode (termed S-LMO), which has undergone approximately 20% Li depletion, as a representative model for an electrochemically aged cathode material. This selection was made to thoroughly examine the intricate changes in the crystal structure and the oxidation state of the Mn element during the process of chemical relithiation. The refined XRD pattern showed that the S-LMO still maintains the spinel phase (Figure 9d), which is consistent with the lattice structure (Figure 9e) of regenerated LMO (R-LMO), but its Li vacancy concentration is about 20%. The changes in S-LMO cell parameters relative to R-LMO can be further obtained. Due to the loss of Li, the lattice parameter within this cubic structure transitioned from a value of a = b = c = 8.23 Å to a reduced dimension of a = b = c = 8.20 Å. They also

analyzed the evolution of the Mn valence state of the S-LMO by XPS. The XPS results for spent and regenerated LMO are shown in Figure 9f and Figure 9g. They found that the Mn valence states on the surface of R-LMO are mainly Mn(III) and Mn(IV), which accounted for 52.72% (Mn^{3+}) and 47.28% (Mn^{4+}), respectively. For S-LMO, a large amount of Mn (IV) appeared on its surface, where Mn^{4+} dominates in S-LMO with a high proportion of 70.22%, owing to charge compensation caused by formed Li vacancies. SEM is used to observe the changes in the surface of cathode materials after cycling. Ren et al. [144]found that the particles of the S-LMO remained intact without cracks (Figure 9h-i). Chen group [141]observed the S-LMO cathodes present a complete lattice structure (surface and bulk), and its crystal lattice does not exhibit structural defects such as distortion or vacancy (Figure 9j). However, the lattice fringe spacing is inconsistent with that of the regenerated cathode, which is attributed to the contraction and expansion of the crystal lattice during cycling. The lattice fringe spacing of the R-LMO cathode is 0.48 and 0.25 nm (Figure 9k) for the corresponding (111) and (311) crystal planes of P-LMO, respectively. This indicates that the types of defects generated on and in cycled LMO may be related to the cycling conditions of the cathode materials. By ameliorating the working conditions of the battery, it is possible to produce easily repairable defect structures and improve the direct recovery efficiency of cathode materials.

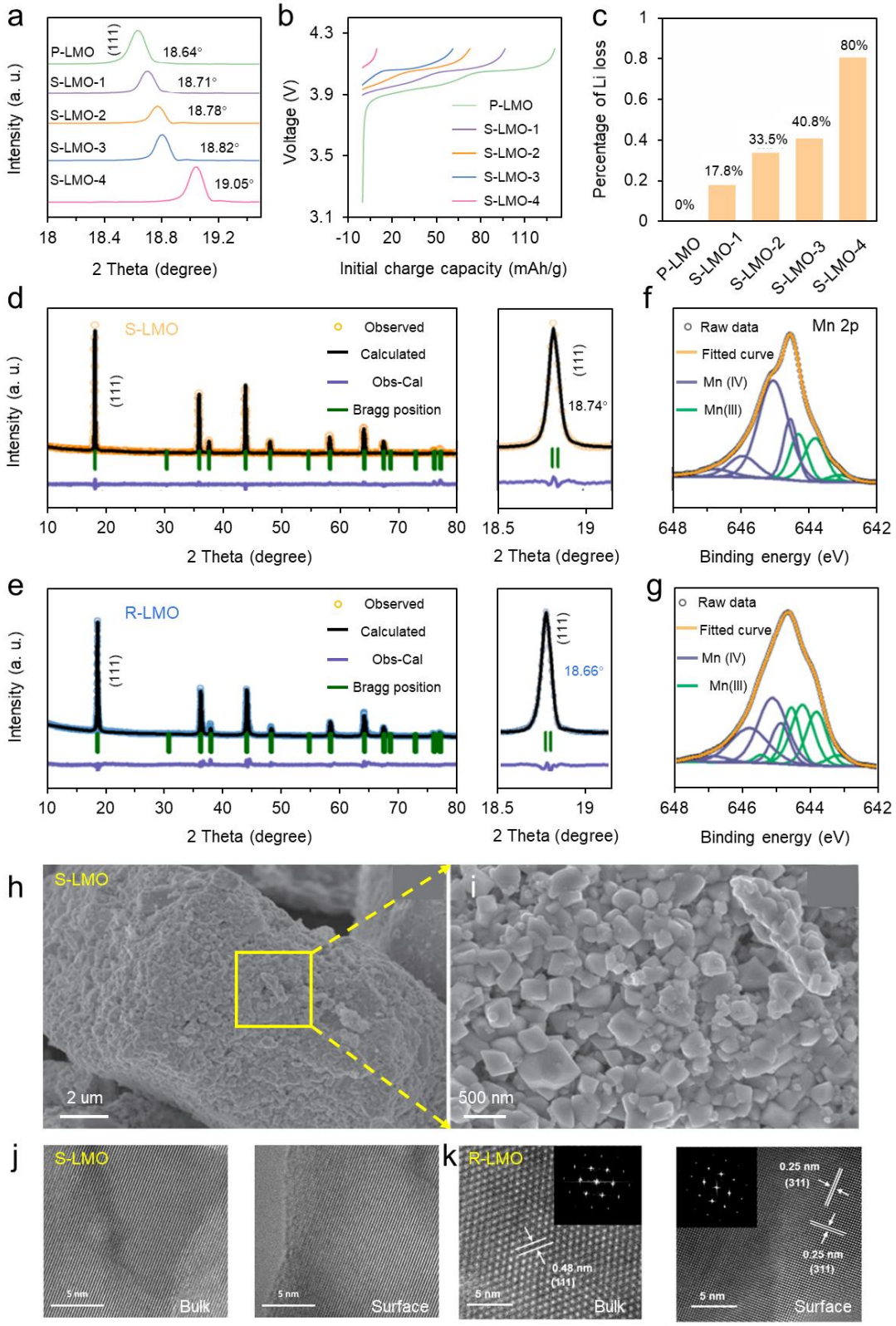

Figure 9. (a-c) XRD patterns, initial charge curves, and ICP results of P-LMO and regenerated LMO samples with different methods. [142] Copyright 2023, Elsevier. (d-e) The Rietveld refinement of S-LMO and R-LMO cathode materials. [142] Copyright 2023, Elsevier. (f-g) XPS results of S-LMO and R-LMO cathode materials. [142] Copyright 2023, Elsevier. (h-i) SEM images and corresponding selected region enlargement of S-LMO. [144] Copyright 2020, The Electrochemical Society. (j)

HRTEM images (bulk and surface) of S-LMO. [141] (k) HRTEM images (bulk and surface) and corresponding fast Fourier transform of R-LMO. [141] Copyright 2020, American Chemical Society.

Li et al. [145] also explored the structure of the spent LMO, which is inconsistent with the results of the above literature. The generated defects of S-LMO may be related to the degree of degradation of materials. They performed XRD on S-LMO, and the results show that the S-LMO contains Mn_3O_4 and Mn_2O_4 impurity phases (Figure 10a), which means that in addition to Li vacancies, Mn_3O_4 and Mn_2O_4 are also the defect types contained in S-LMO. The SEM image of S-LMO after multiple cycles shows obvious cracks on the surface of the particles (Figure 10b and Figure 10c), reflecting the damage by the repeated shrinkage and expansion of the lattice structure during the charging and discharging process. The reason for the formed crack on S-LMO is similar to the cause of generated cracks on the surface of the lithium cobalt oxides and ternary cathode materials. [69,146,147] Peng et al. [148] discovered that the S-LMO possesses a highly ordered structural domain with lattice fringe spacing of 0.47 nm, which aligns with the (003) crystal plane of the LMO. [149] They also found that the spent cathode had distinct disordered regions, amorphous phases, and corrosion holes in addition to the structure of the spinel LMO (Figure 10d and Figure 10e). During the cycling process, these undesirable phases, which exhibit no electrochemical activity, cause a diminishment of capacity and an increasement in impedance. [150,151] The formation of these unfavorable phases is closely related to the Jahn–Teller effect of Mn and considerable Mn dissolution during cycling. The presence of Mn primarily in the form of Mn^{3+} dissolved in the electrolyte was confirmed by Amine et al.[152] In summary, after long-term cycling, the LMO tends to have Li vacancies and Mn_3O_4 and Mn_2O_4 impurities phases, which inevitably affect discharging capacity and cycle life. For spent LMO, in addition to the formed above-mentioned defects, Mn^{3+} undergoes a disproportionation reaction and forms $Li_4Mn_5O_{12}$ and soluble Mn_3O_4 during the initial charge process. During the discharge process, LMO formation occurs accompanied by the Jahn-Teller distortion, particularly nearing the completion of the lithiation stage. [152] Chen et al.[141] did not find the Mn_3O_4, Mn_2O_4 impurities phase, amorphous phase, and corrosion hole in spent LMO, which possibly due to the materials or cycling protocols discrepancy. It is worth

noting that there is no unified conclusion on the failure mechanisms of LMO cathodes after long cycle, and further research is needed to shed more light on the degradation mechanism. [1]

Direct regeneration of spent LMO

Although researchers have carried out tremendous research on LMO, the degradation mechanisms of LMO are still in the exploration stage, and the related reactions involved in the regeneration process are not discussed here. The main direct regeneration method of spent LMO is solution-based direct recycling approach.[141,142,153] Chen et al. [141] used LiOH solution with different concentrations to repair the spent LMO by hydrothermal treatment (Figure 10f). The appropriate LiOH concentration (like 0.1 M) could effectively repair Li vacancies in spent $Li_2Mn_2O_4$, and the repaired LMO showed excellent performance as the pristine LMO. During regeneration, they found the higher LiOH concentration (like 0.4 M) will induce Li-rich phase LMO impurities, and lower LiOH concentration (like 0.02 M) cannot adequately and effectively repair spent $Li_2Mn_2O_4$ during the lithiation process. Qian et al. [142] designed a green and inexpensive method to regenerate spent LMO at room temperature. They used Pyrene-Li solution as a lithium source, and the Li vacancies in spent LMO could be repaired by stirring the spent LMO with Pyrene-Li solution at room temperature. Spent LMO can be repaired as pristine LMO cathodes with comparable long-term cycling stability. At present, researchers have limited research on the direct regeneration of spent LMO compared to LCO, ternary cathode or LFP, on the one hand, because LMO has not been popularized on a large scale, the acquisition of spent LMO is not as convenient as these cathodes that have been commercialized. Most importantly, there is very limited understanding for the defect formation during cycling.

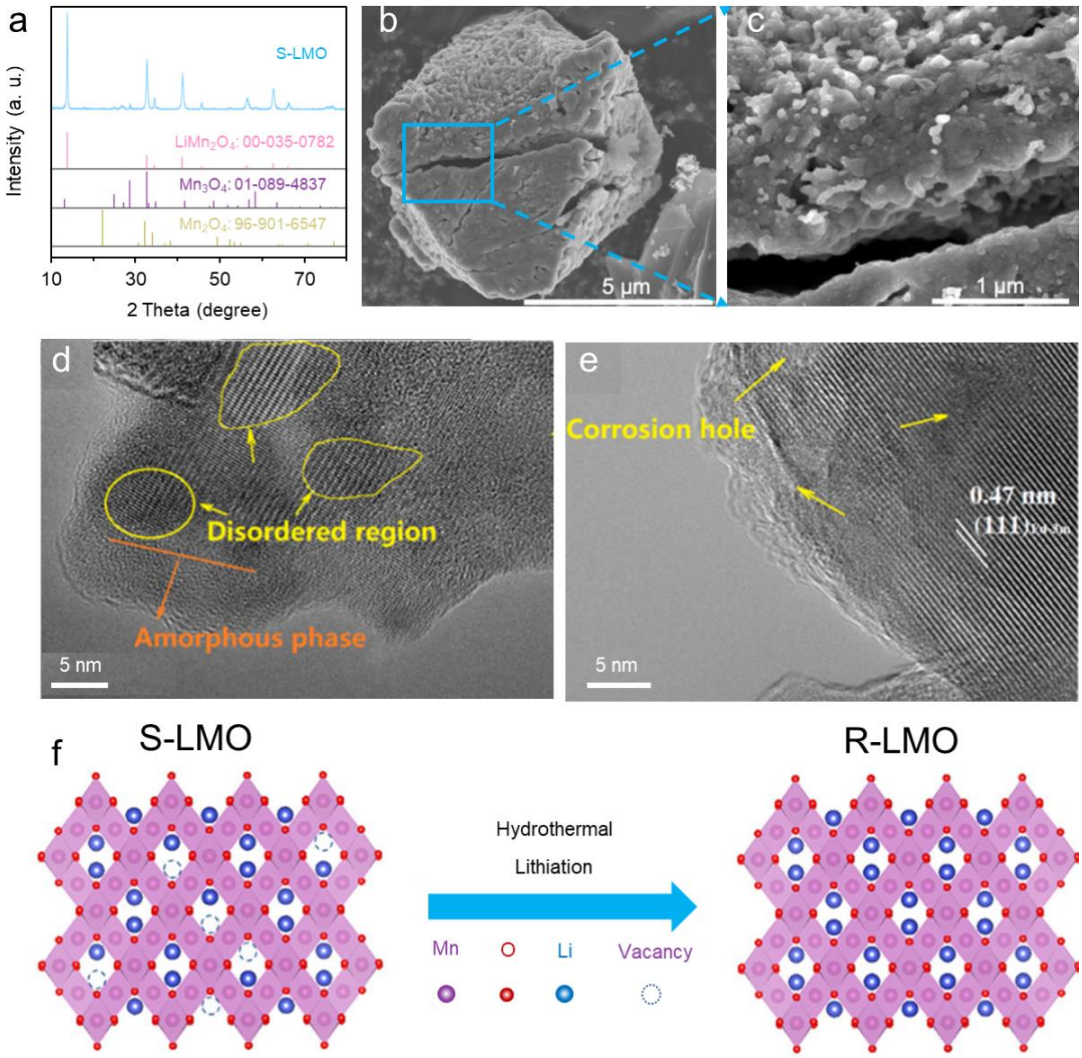

Figure 10. (a) XRD patterns of S-LMO. [145] Copyright 2022, WILEY-VCH Verlag GmbH & Co. (b, c) SEM images and corresponding local region enlargement of S-LMO. [145] Copyright 2022, WILEY-VCH Verlag GmbH & Co. (d, e) HRTEM images of S-LMO. [148] Copyright 2019, Elsevier. (f) Schematic of regenerating S-LMO by hydrothermal treatment. [141] Copyright 2020, American Chemical Society.

In this review, we focus on analyzing the failure mechanisms of four types of cathode materials ($LiCoO_2$: LCO, $LiNi_xCo_yMn_zO_2$ (x+y+z=1): NCM, $LiFePO_4$: LFP, $LiMn_2O_4$: LMO) and the defective structures in these degraded cathode materials. Different defective structures require different regeneration environments, specifically as follows.

For degraded layered cathodes (LCO and NCM), at the micron or sub-micron scale, their particle surfaces exhibit noticeable cracks; at the nanoscale, the surfaces of the degraded layered cathode particles are characterized by rock salt and spinel structure. For the bulk of failed layered cathode material, the particles consist of layered structures

with substantial amount of lithium vacancies. The aforementioned defective structures can be transformed into layered cathode materials under suitable lithium-rich conditions. It is worth noting that due to the evident similarities of defective structures in layered cathode, there is no significant distinction between the environmental conditions and repair methodologies employed in their restoration process. This also explains why a single method reported in the literature is capable of simultaneously regenerating spent LCO and NCM cathodes. [50,87]

Spent LFP particles generally do not display evident cracks at the micron scale. However, at the nanoscale, spent LFP can exhibit the generation of new phases ($FePO_4$: FP), leading to phase segregation in its microstructure. Consequently, the spent LFP particles manifest a coexistence of both LFP and FP phases. In addition, spent LFP can also exhibit Li/Fe anti-site defects in its structure. For the repair of the FP phase, an appropriate lithium-rich condition is required, while the restoration of Li/Fe anti-site defects necessitates a reducing environment, as a reducing atmosphere can overcome the electrostatic repulsion that impedes Fe from returning to its original sites. Therefore, for the direct regeneration of spent LFP, besides the need for re-lithiation under suitable lithium-rich conditions, providing a reducing environment is also essential.

Research into the failure mechanisms and recovery strategies for LMO is still insufficient, with current findings indicating that the restoration of LMO typically necessitates an appropriate suitable lithium-rich condition.

In both suitable lithium-rich environments and reductive environments, these methods (solid-state sintering, molten salt lithiation, solution lithiation, electrochemical lithiation, and ionic liquid lithiation) can be employed to achieve the desired outcome.

The specific methods employed for the rejuvenation of degraded cathode materials include solid-state sintering, molten salt lithiation, solution lithiation, electrochemical lithiation, and ionic liquid lithiation (Table 2).

Solid-state sintering involves elevated temperatures during the process of repairing cathode materials. This process leverages heat to drive diffusion and bonding between solid particles, thereby restoring or enhancing the performance of the cathode material.

Molten salt lithiation allows for the reduction of the relithiation temperature during regeneration. The selection of different types of molten salts can provide distinct environments for the repair process, such as a reducing atmosphere or an oxidative environment, thus tailoring the conditions according to the specific requirements for rejuvenating the performance of the spent cathode.

Solution lithiation generally requires high-pressure conditions, making the repair process more complex. Nonetheless, during the repair process, lithium ions in the solution can diffuse more uniformly into the interior of the cathode material, contributing to the formation of a homogeneous and complete lithiated structure, which enhances the efficiency of cathode material restoration.

Electrochemical lithiation can repair defect structures in spent cathode materials mainly by featuring lithium vacancies, and it does so under mild conditions without necessitating a high-temperature process.

During the cathode repair process using ionic liquid lithiation, the ionic liquid hardly evaporates, which minimizes environmental pollution and safety hazards. However, the cost of ionic liquids is notably higher.

In summary, each method has its advantages and disadvantages during the direct regeneration of spent cathodes, and the specific choice of methodology is required to be closely related to the degradation degree of cathodes.

Table 2. Regeneration methods, conditions, and performance of cathode materials reported in the literature.

	Regeneration condition	Performance
LCO regeneration method		
Solid-state sintering	Spent LCO cathode + Li_2CO_3(molar ratio of Li/Co:1.05), sintering at 850–950 °C for 12 h in air [76]	152.4 mAh g^{-1} at 30 mA g^{-1} (0.1C), 98.35% capacity retention after 100 cycles
Electrochemical lithiation	Three electrodes system, 0.3 M Li_2SO_4 electrolyte, 0.42 mA cm^{-2}, sintering at 700 °C for 2 h in air [79]	136 mAh g^{-1} at 0.2C, no significant decay of capacity after 200 cycles
Solution lithiation	D-LCO+ 4 M LiOH, hydrothermal at 220 °C for 4 h, sintering at 850 °C for 4 h [81]	148.2 mA h g^{-1} at 1C, 91.2% capacity retention after 100 cycles
Eutectic lithiation	S-LCO+ LiCl–CH_4N_2O solvent at 120 °C, sintering at 850 °C for 2 h [65]	130 mAh g^{-1} at 0.1C, 90% capacity retention after 100 cycles
Spent $LiNi_xCo_yMn_zO_2$ (x+y+z=1) regeneration method		
Solid-state sintering	S-NCM111+ Li_2CO_3 (ball milling at 500 rpm, 4 h), Li/Mn=1.2, sintering at 800 °C for 10 h in air [103]	165 mAh g^{-1} at 0.2C above 80% capacity retention after 100 cycles
	S-NCM523+ Li_2CO_3(molar ratio of Li/Co:1.05), sintering at 850 °C for 12 h in air [100]	162 mAh g^{-1} at 0.1C, 91.9% capacity retention after 100 cycles at 1C
	Peroxidation with $Na_2S_2O_8$ and NaOH, D-NCM622+ $LiOH·H_2O$(molar ratio of Li/Co+Ni/Mn:1.05), sintering at 850 °C for 5 h in O_2 [102]	153.82 mAh g^{-1} at 1C, 94.74% capacity retention after 100 cycles at 1C
Solution lithiation	0.2 g S-NCM523 +20 mL NH_4OH, hydrothermal at 180 °C for 6 h(HS-NCM523), 0.1 g HS-NCM523+ 18 mg LiOH, sintering at 500 °C for 2 h, followed by 10 h at 850°C in air [50]	~152 mAh g^{-1} at 0.5 C, ~90% capacity retention after 100 cycles and ~76% capacity retention after 200 cycles at 0.5C

Molten salt lithiation	D-NCM523+ 4 M LiOH, hydrothermal at 220 ℃ for 3 h (P-HT-3h), 2.3 g P-HT-3h +0.12g $LiOH·H_2O$, sintering at 810 °C for 4 h in O_2 [105]	90.8% capacity retention after 500 cycles with the mass loading of cathode around 21 ± 0.5 mg cm^{-2} in pouch cell (1.7 Ah)
	S-NCM523: LiI-LiOH (molar LiOH / (LiI + LiOH) = 0.45)=1:3(molar ratio), adding 5 wt% Co_2O_3 and MnO_2 of S-CM523, sintering at 200°C for 4 h followed by 5 h at 850°C [87]	Comparable to that of the C-NCM523, more than 80% capacity retention after 200 cycles and 73% after 300 cycles
	1 g D-NCA+0.84 g $LiOH·H_2O$ +0.56 g Na_2SO_4. sintering at 750 °C for 5,10,15 h in air [51]	204.8 mAh g^{-1} at 0.1C, 85.1 % capacity retention after 250 cycles at 1C
Ionic liquid lithiation	2.5 mmol D-NCM111+2.5 mmol LiCl+ 2.5 mL [C2mim] [NTf2], heating at 150–250 ℃ for 6–24 h [45]	173.6 mAh g^{-1} at 0.1C
LFP regeneration method		
Solid-state sintering	Spent LFP + Li_2DHBN (5 wt%), sintering at 800 °C for 6 h in Ar/H_2 [2]	157 mAh g^{-1} at 0.1C, 88% capacity retention after 400 cycles at 5 C
Electrochemical lithiation	D-LFP+$Li_2C_2O_4$/CMK-3 Prelithtiated separator [6]	152 mAh g^{-1} at 1C, 83.5% capacity retention after 150 cycles at 1 C, 146.7 mAh g^{-1}, 90.7% capacity retention after 292 cycles in D-LFP/graphite full cell
Solution lithiation	100 mg D-LFP+10 mg PVP+15 mg CH_3COOLi+15 mL ethanol, hydrothermal at 180 °C for 5 h, Sintering at 700 °C for 5 h in Ar [52]	145.7 mA h g^{-1} at 1C, 85.2% capacity retention after 500 cycles
Molten salt lithiation	S-LFP: $LiNO_3$:FeC_2O_4=1:0.5:0.1(molar ratio), heating at 300 °C for 2 h, sintering at 650 °C for 6 h in Ar[128]	145 mAh g^{-1} at 0.5C, over 90% capacity retention after 100 cycles

	D-LFP+0.2 M Li^+ solution (prepared by graphite), dring at 80 °C for 8 h and annealing at 600 °C Ar for 2 h in Ar [109]	157.4 mAh g^{-1} at 0.1C, without an apparent sacrifice of capacity retention after 200 cycles
LMO regeneration method		
Solution lithiation	0.25 g of cycled LMO+80 mL 0.1 M LiOH, heating at 180 °C for 12 h [141]	111 mAh g^{-1} at 0.5C, 88.2% capacity retention after 100 cycles at 5 C
	D-LMO:Py-Li/DME(0.05M)=1:1 (molar ratio), stirring 30min [142]	123.4 mAh g^{-1} at 0.1C, 92% capacity retention after 150 cycles at 0.5C

Degradation mechanisms of graphite anode and the corresponding characterization methods

Graphite is the most commonly used anode material for LIBs due to its high electrical conductivity, high thermal and mechanical stability, ultralong cycle life, good capacity, and low operating voltage. [154-156] Zhang et al. [157] observed that spent graphite (SG) has a defective structure with a rough surface (Figure 11a and Figure 11b) compared to the pristine graphite surface, which is attributed to the side reactions between the graphite surface with the electrolyte during the electrochemical cycle.[158-161] In addition, small detached and broken fragments could be observed on the surface of SG, which is caused by the continuous change of graphite interlayer distance during the process of Li^+ intercalation, deintercalation, or continuous growth of lithium dendrites). [115,162-164] Through the XRD pattern analysis of SG, Liao [165] found that its phase is still graphite, showing the characteristic diffraction peaks of the (002), (100), (101), (102), and (110) crystal planes of graphite, but two weaker diffraction peaks appear around 20° and 30° (Figure 11c), which are related to binders on SG surface or excessively thick solid electrode interphase (SEI) formed during cycling. These structures or defects are one of the main factors for the capacity fade of graphite during cycling. [166-169] The samples (regenerated graphite (D-RG) obtained by deep eutectic solvent treatment and the regenerated graphite (H-RG) obtained by H_2SO_4 leaching) do not show any amorphous peak, indicating the method with deep eutectic solvent and acid leaching can effectively remove impurity on the surface of SG. They further explored the surface composition of SG through XPS, In the SG, the chemical bonding involving F elements consisted of P-F bonds, LiF bonding, and the repetitive unit of perfluoroalkyl chains $(-CH_2CF_2-)_n$. (Figure 11d), which is derived from the Li salt components in the electrolyte, SEI, and organic binders, respectively. Upon detailed analysis, the C atomic species within the SG sample could be separated and matched to six distinctive peaks, reflecting various chemical environments: $(-CH_2CF_2-)_n$, O–C=O, C–O, C–OH, C–C, and C, respectively. (Figure 11d). Among them, C comes from the inherent layered C-six-membered ring structure maintained in SG, and the other chemical bonding combined with C mainly comes from organic binders, SEI, or

impurities formed on the surface of SG. The regenerated graphite (D-RG and H-RG) showed a significant reduction in impurity composition and recovery of the graphite structure (Figure 11d). TEM characterization was performed on SG by Wang et al. The results showed that the surface of SG was dominated by an amorphous structure with uneven thickness, which was attributed to the organic binders or generated SEI during cycling, and the surface of regenerated graphite (RG) showed an obvious layered structure (Figure 11e). In-situ Raman analysis was used to evaluate the formation of the defect repair during the regeneration process. As can be seen from Figure 11f, the SG shows a high I_D/I_G ratio compared with that of RG, this suggests that the layered configuration of graphite has been destroyed throughout the cycling process. [170-172] The anodic process could be affected by the cathodic reaction products during the life of the electrochemical cell. Taking graphite paired with NCM cathode as an example, the transition metal ions dissolved from the cathode were reported to be deposited on the surface of the graphite during cycling, which deteriorate the electrochemical performance of the anode and cell. [173-175] Klein et al. [176] conducted elemental analysis on the cycled graphite, and the results showed apparent signs of Ni, Co, and Mn elements in the cycled graphite (Figure 11g). These transition metal elements deposited on the surface of graphite can accelerate the catalytic decomposition of the electrolyte, which in turn affects the cycle of the battery. In addition to the above impurities, defects, SEI, or organic binder in SG, Wang et al. [40] found that the SG just disassembled from the battery has a golden yellow colour, indicating a large amount of LiC_x on the surface. These substances do not convert into active Li^+ during the charging and discharging process and remain on SG. They have even been reported to be toxic to normal intercalation and deintercalation of Li^+.[1,177] Therefore, the presence of LiCx in and on SG was concluded to be another reason for the capacity fade of LiBs. In summary, spent graphite includes defective structures formed on the surface of graphite, trapped Li (LiC_x), SEI, organic binders, and impurities (deposited Ni, Co, Mn on the surface of graphite), [160,165,178-181] which need to be repaired or removed during direct regeneration.

Direct regeneration of spent graphite

Based on the above discussion, strategies for the direct recycling of graphite need

to consider defective structures, LiC_x, SEI, organic binders, and impurities (deposited Ni, Co, Mn on the surface of graphite) on the surface of graphite. [182-187] Wang et al. [40] mixed the SG that had just been collected from the disassembled battery with water to utilize the highly reactive properties of LiC_x with water to remove trapped Li in SG and eventually converted them into Li_2CO_3, which can be further used for the regeneration of spent cathode. The (002) crystal plane spacing of the graphite with removed LiC_x by water is almost the same as that of the RG (Figure 11e), indicating the change in graphite layer spacing may be related to the formed LiC_x during cycling. Regenerated graphite was reported to achieve a 370 mAh/g capacity after annealing the LiC_x-free SG, which is comparable to the pristine graphite. The James M. Tour team [188] developed a rapid, efficient, low-carbon regeneration method for graphite anodes. They used a fast joule heating process to direct regenerate spent graphite, which increased the temperature of SG to 2850 K in less than 0.2 seconds, breaking down the SEI and binders while maintaining the morphology of graphite, ultimately achieving efficient repair of SG. The so-called flash-recycled anode demonstrated a restored specific capacity of 351.0 mAh/g at 0.2C, along with robust electrochemical stability. When paired with a $LiFePO_4$, it maintained a commendable capacity retention of 77.3% even after undergoing 400 cycles at 0.5C. Huang et al. [189] used impact heating (1500 °C, 1 second) and continuous rolling heating (~5 m/min) to efficiently regenerate SG. This used shock-type heating decomposed the organic binder into amorphous carbon layers and gases (Figure 11h). SG was initially subjected to purification via treatment with 2 M H_2SO_4 solution for a duration of 1 hour at ambient temperature, aimed at eliminating superficial contaminants. Following thorough rinsing with distilled water and subsequent drying, the cleansed graphite was subsequently coated with polyacrylonitrile (PAN) and then thermally decomposed under an argon atmosphere at a temperature of 1100 °C, thus yielding RG with minimal surface imperfections. The RG by this method was able to match the performance of pristine graphite with 340 mA h/g at 0.5C initial capacity and capacity retention >98% after an additional 180 cycles. As for the transition metals deposited on the surface of spent graphite, Zhang et al. [190] found that H_2SO_4 can effectively remove the remaining transition metals from dissolved

cathodes in spent graphite. After the sulfuric acid curing and leaching process, RG was obtained by sequential calcination at 1500 °C. The rejuvenated graphite showcased excellent electrochemical attributes, manifesting in commendable charge capacity and stable cycling performance. It delivered an initial charge capacity of 349 mAh/g.

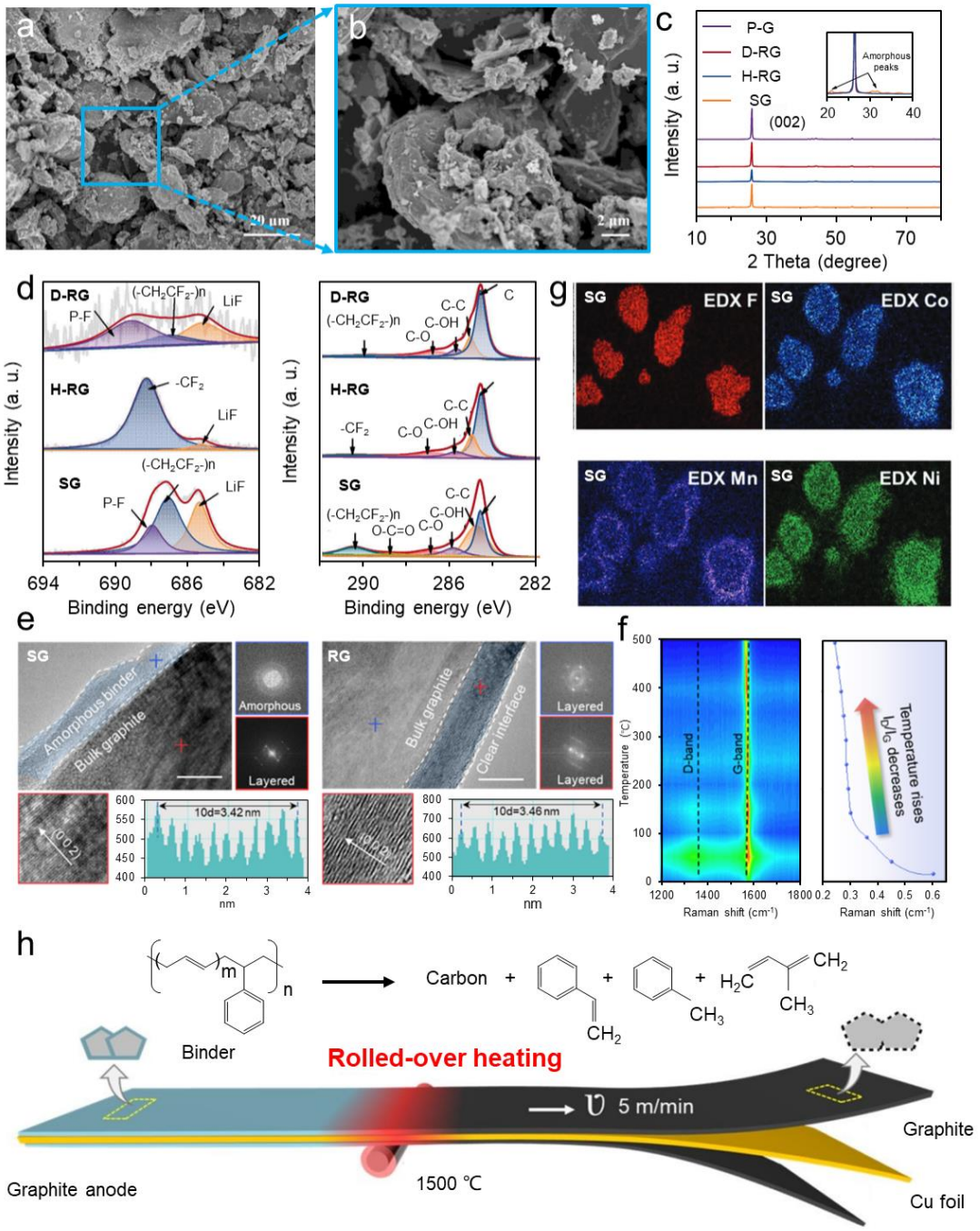

Figure 11. (a, b) SEM images of SG. [157] Copyright 2023, Elsevier. (c) XRD patterns of P-G, SG, and regenerated graphite (D-RG, H-RG) with different methods. [165] Copyright 2022, Elsevier. (d) XPS results of S-G, D-RG, H-RG. [165] Copyright 2022, Elsevier. (e) TEM and HRTEM images of SG and RG. [40] Copyright 2022, American Chemical Society. (f) The evolution of Raman spectra

during the process of repair SG. [40] Copyright 2022, American Chemical Society. (g) SEM-EDX images of SG. [176]Copyright 2021, WILEY-VCH Verlag GmbH & Co. (h) Schematic of transient recycling of spent graphite from copper foils via rolled-over heating. [165] Copyright 2023, Royal Society of Chemistry.

Degradation mechanisms and direct regeneration of used current collector

The recycling of spent LIBs has been widely acknowledged as a practical and effective measure to confront the burgeoning problem of LIB waste. Although most recycling research initiatives have largely centered on reclaiming the active electrode materials, there exists a relative dearth of focus on the inactive parts of the battery, such as the current collectors. These collectors are typically embodied by aluminum and copper foils, which cumulatively constitute over 15% of the overall weight of LIBs. [191-193] Efficient recycling of current collectors holds promise for significantly reducing LIB waste, simultaneously furnishing a sizeable secondary supply of Al and Cu resources. [191,194-196] However, at present, there is very little research on the direct regeneration of current collectors. Kendrick's group claims [197] that they were the first to regenerate exhausted current collectors directly. Based on their research, we analyzed the defects in cycled current collectors and the direct regenerate methods of current collectors.

Kendrick et al. [197] disassembled the spent battery and the current collectors by physically separating the electrodes' active materials (Figure 12a). The retrieved positive current collector made of Al is straightforwardly processed with NMP until the point where no evident black film is visually detectable on its surface. (Figure 12b). They found that the obtained Al by the above method has obvious craters and rolling or calendering traces on the surface (Figure 12d) compared to the smooth surface of pristine Al (Figure 12c). The used Cu is cleaned with water and HCl (Figure 12b), and after washing, the copper surface exhibits a predominantly smooth and unblemished appearance, save for a few instances of corrosion pits and cracks. (Figure 12g) compared to the pristine Cu presenting a smooth surface (Figure 12f). They showed that the Al or Cu current collector maintained the initial morphology of the used current collector after cleaning. And some defects, such as cracks or holes on the surface of the current collector, this could potentially stem from the interaction between the current collector and electrolyte during the charging and discharging process. [198-202] They repair

and regenerate the used current collector by further acid etching (Figure 12b), and the repaired current collector exhibits a rougher surface (Figure 12e and Figure 12h). They characterized the used Al and Cu current collectors with XPS, where Al 2p spectra showed that the Al oxide characteristic peak intensity of the regenerated Al collector by etching was greater than that of the Al oxide of the cleaned current collector (Figure 12i). This is due to the F-containing residue on the used Al current collector surface being removed by etching, which was verified by the XPS results of F1s. [197] Similarly, the O1s results of Cu also show residue on the surface of the used Cu current collector is removed by etching (Figure 12j). They also found that the regenerated Al and Cu current collectors have greater adhesion strength between electrodes and current collectors (Figure 12k and Figure 12l). The regenerated current collectors by the proposed method show electrochemical performance similar to that of the pristine one at low C rates.

The researchers also studied the functionalization of used current collectors besides the direct regeneration of used current collectors. Vanchiappan Aravindan et al.[203] reported a simple and effective method to upcycle copper current collectors from spent LIBs and into CuO anodes for sodium-ion batteries. They further paired them with carbon-coated $Na_3V_2(PO_4)_2O_2F$ cathode into a full cell, which displayed good capacity retention with a Coulombic efficiency of >95% from the second cycle. Li et al. [204] converted the used Al current collector and the spent LCO into $LiNi_{0.8}Co_{0.15}Al_{0.05}O_2$ (NCA) cathode, which delivered an initial discharge capacity of 215.28 mAh/g and maintained roughly 80% of its capacity after enduring 180 cycles. Fei et al. [205]proposed a two-step technique for the direct revitalization of spent ternary cathode materials. Within this methodology, they employed aluminum impurities sourced from discarded current collectors to compensate for missing transition metals, thereby facilitating simultaneous elemental substitution and structural repair. The regenerated ternary cathode materials with controllable Al doping delivered outstanding cycling performance (89.6% capacity retention, 200 cycles). At present, the recovery of the current collector mainly focuses on the functionalized application of the used current collector, and there exist relatively sparse research endeavors dedicated to

the direct regeneration of current collectors.

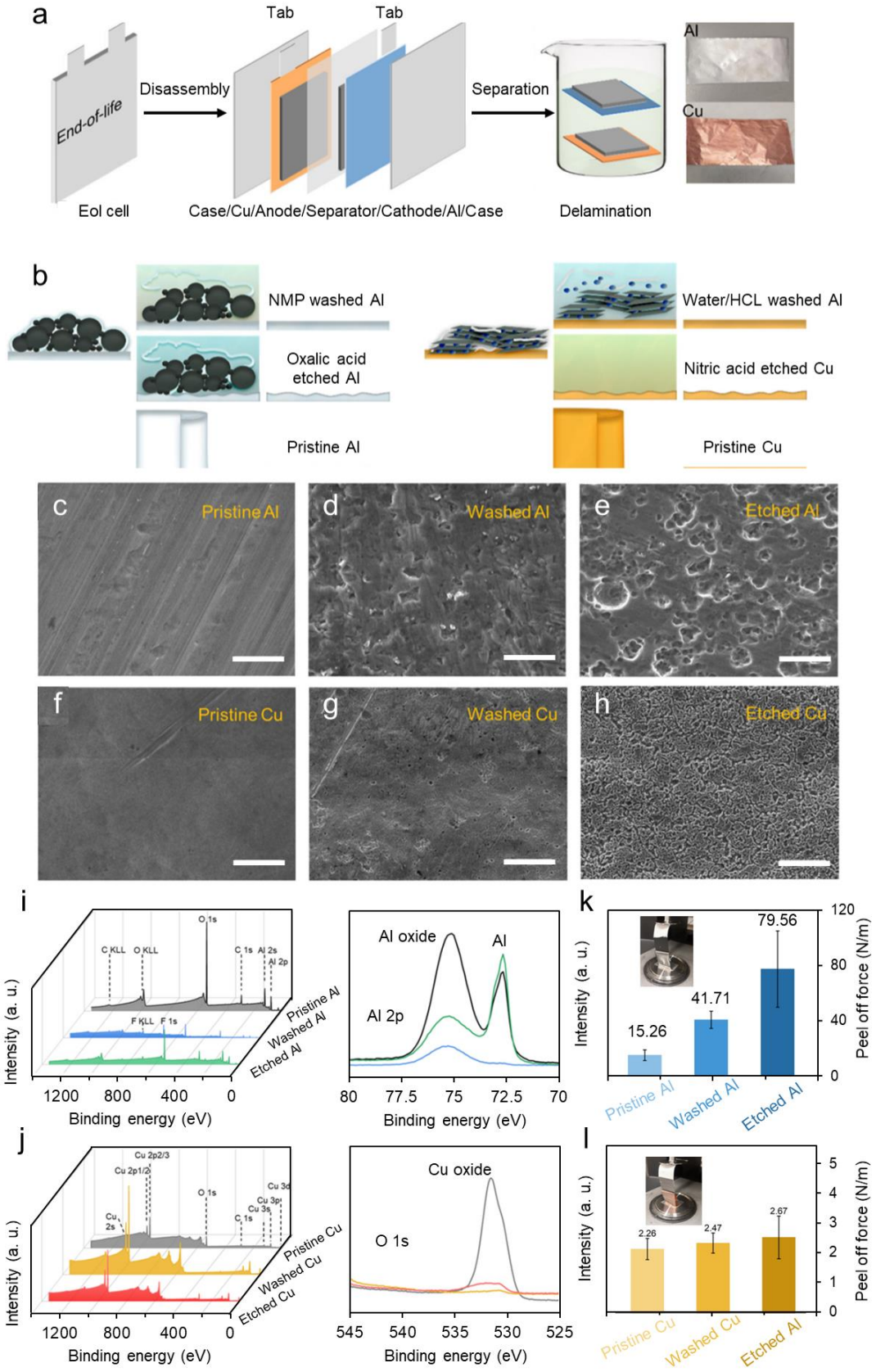

Figure 12. (a) Reclamation of Al and Cu current collectors from end-of-life lithium-ion battery cells. (b) different treatments for electrode delamination from current collectors. (c-e) SEM images of

pristine Al, washed Al, and etched Al. (f-h) SEM images of pristine Cu, washed Cu, and etched Cu. (i-j) XPS results of different samples. Peel off force between (k) Al current collectors and electrodes and (l) Cu current collectors and graphite electrodes. Reproduced with permission. [197]Copyright 2023, Royal Society of Chemistry.

The feasibility of direct regeneration processes in terms of environmental impact, energy consumption and economic benefit.

We take the recycling of widely used layered cathode material, lithium cobalt oxide (LCO), and olivine structured cathode material, lithium iron phosphate (LFP), as examples to illustrate the feasibility of direct regeneration of spent cathodes in comparison to conventional hydrometallurgical (hydro) and pyrometallurgical (pyro) recycling methods, when considering factors such as environmental impact, energy consumption, and economic benefit.

Cheng et al. [53]doped Al/Mg elements into the spent cathodes during the process of regeneration. Ultimately, they produced a regenerated high-voltage LCO cathode material with stable cycling at 4.6 V by the solid-state sintering method. The flowchart for the direct regeneration of spent LCO cathodes is depicted in Figure 13a. Taking the recycling of 1 ton spent LCO lithium-ion batteries as an example, after disassembling the batteries and removing components such as separators, anodes, and battery casings, approximately 0.498-ton LCO cathode sheets were obtained. These cathode sheets were then subjected to N-Methyl-2-pyrrolidone (NMP) treatment, which facilitated the separation of the active material from the current collector, resulting in 0.298-ton LCO cathode material. Subsequently, the spent LCO cathode material was converted into a high-voltage LCO cathode by solid-state sintering process. Compared to traditional hydrometallurgical and pyrometallurgical recycling methods for spent LCO, direct regeneration demonstrates a higher integrated advantage (Figure 13b) including Greenhouse Gas (GHG) emission. Taking into account the costs of materials, energy consumption, and environmental impacts such as greenhouse gas emissions, the direct recycling process still yields a profit of 3,671.3 $ (Figure 13e), which significantly surpasses the profits generated by hydrometallurgical and pyrometallurgical recycling methods (Figure 13c, Figure 13d), emphasizing the greater economic and environmental benefits of direct recycling for spent LCO cathodes.

As for the regeneration of spent LFP, Chen et al. [49]employed hydrothermal methods to directly repair spent LFP cathode materials. In their study, they simulated the energy consumption and greenhouse gas emissions associated with various recycling processes for LFP. Their findings revealed that direct recycling exhibited the lowest energy consumption and greenhouse gas emissions among the evaluated methods (Figure 13f, Figure 13g). They also conducted simulations on the costs and benefits associated with different recycling methods. Their results showed that the costs of hydrometallurgical and pyrometallurgical recycling of spent LFP are indeed significantly higher than their corresponding benefits (Figure 13h). This is a key factor contributing to the reluctance of today's industry to extensively recycle LFP cells. The situation might be attributed to the fact that LFP contains only lithium as a relatively precious metal element. There is a clear advantage of direct recycling methods for spent LFP in terms of economic benefits (Figure 13i). Zhou et al. [2]conducted a simulation on the economic benefits of recycling spent LFP cathodes. According to their results, the hydrometallurgical recycling process, due to its complex process requiring substantial human labor and large-scale equipment, incurs notably higher recycling costs (Figure 13j). Consequently, this method does not generate positive economic returns (Figure 13k). On the contrary, direct recycling of spent LFP demonstrates a significant economic benefit (Figure 13k), reinforcing the rationale behind adopting direct recycling methods for the recovery of spent LFP cathode materials.

In summary, taking into account the environmental impact, energy consumption, and economic benefit, direct recycling exhibits more pronounced comprehensive advantages over traditional hydrometallurgical and pyrometallurgical recycling methods and direct recycling emerges as a more environmentally friendly and economically feasible strategy for the recycling of spent lithium-ion battery.

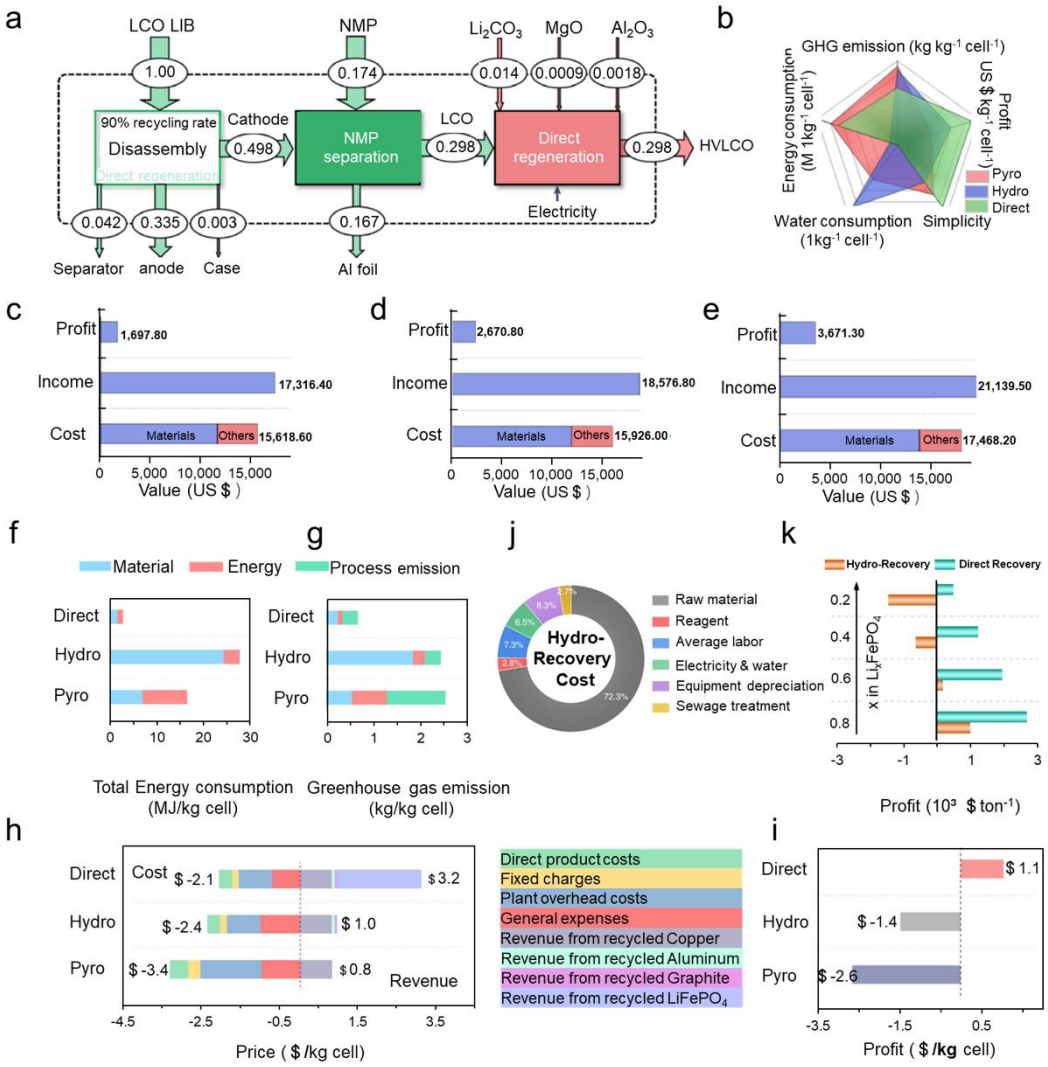

Figure 13. (a) A flowchart illustrating the direct recycling process for spent LCO. (b) Comprehensive comparison of different recycling strategies. (c) Economic analysis of the pyrometallurgical recycling process for spent LCO. (d) Economic analysis of the hydrometallurgical recycling process for spent LCO. (e) Economic analysis of the direct recycling process for spent LCO [53]. Copyright 2023, Springer Nature Limited. (f) Total energy consumption analysis of different recycling methods for spent LFP. (g) Greenhouse gas emission of different recycling methods for spent LFP. (h, i) Cost and profit of different recycling methods for spent LFP [49]. Copyright 2020, Elsevier. (j) The cost of hydrometallurgical recycling process for spent LFP. (k) Profit of different recycling methods for spent LFP [2]. Copyright 2023, Springer Nature Limited.

Perspective

LIB recycling is a very effective strategy to alleviate the environmental pollution caused by spent batteries and resource sustainable development issues. The direct regeneration method of spent LIBs has a simpler operation process, lower energy input, smaller environmental pollution, and higher value benefits than traditional hydrometallurgical and pyrometallurgical recycling technology. Despite the initial

success achieved in the direct recycling of cathode, anode, and current collector materials, there are still many challenges to realizing large-scale production of recycled materials with high yields. The spent cathode materials to the ready-to-use materials have gone through roughly four steps by direct regeneration, where the first step is detecting the type of degraded cathode and the amount of residual lithium in the cathode (Figure 14a). The subsequent stage entails the proficient detachment and separation of the active materials from the current collectors. (Figure 14b). The third process is analyzing the degraded structure of the cathode (Figure 14c), and the last step is the direct regeneration of the failed cathodes (Figure 14d). The challenges for the whole procedure of the direct regeneration of spent LIBs are summarized as follows.

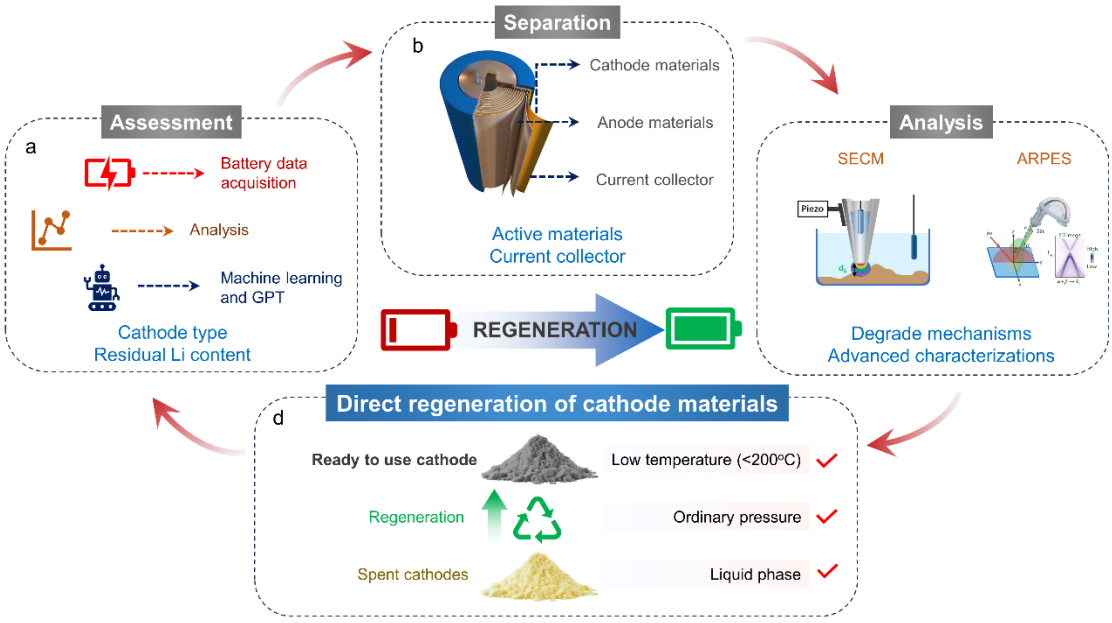

Figure 14. (a) The detection of the type of degraded cathode and the amount of residual lithium in cathode by machine learning and Generative Pre trained Transformer (GPT). (b) Efficient separation of the active materials and the current collector. (c) The analysis of the degraded structure of cathode by advanced characterization [206]. Copyright 2023, 2022, Springer Nature Limited. (d) The regeneration of spent cathodes in the liquid phase environment at low temperature (<200 °C) and ordinary pressure.

1. The lithium replenishment is an important step in the direct repair process of the spent cathode, and the amount of lithium for replenishment is closely related to the residual lithium amount in the spent cathode. According to current literature reports, the residual lithium content in the cathode is determined by ICP measurement, which

is a complex process. In addition, different repair methods are suitable for different cathodes. However, the type of failed electrode materials is also determined by ICP results, which have the same problem encountered in measuring the residual lithium content of the failed cathode. Fortunately, alternative approaches may be available. Different types of cathode materials with different degradation degrees have unique electrochemical characteristics such as charging and discharging curves, voltage, interface impedance, overpotential, etc. Therefore, combining machine learning and artificial intelligence methods such as GPT to analyze and summarize the characteristic data of different types of cathode materials with different degradation degrees is possible. In this way, the cathode type and residual lithium can be determined by measuring the electrochemical data of spent LIBs.

2. At present, the direct regeneration of spent cathodes is almost for the repair and recycling of one type of spent cathode material. However, in practical production, we get a mixture of various spent cathode materials, such as the ternary cathode, LFP, and LCO mixed, and it is difficult to regenerate materials mixed with different types of spent cathode materials. Therefore, developing a direct regeneration method that can be applied to different types of spent cathodes is very critical and necessary to achieve large-scale production of regenerated cathode materials.

In addition, the separation technology of active substances and current collectors (or cathode and anode materials) is not very mature, and the obtained cathode materials often contain impurities (graphite, Cu and Al), which will have a fatal impact on the repaired process. In most of the current methods of direct recycling cathode, the cathode materials and the current collector are separated manually rather than by a machine. Therefore, the pre-separation technology needs to be upgraded before direct repair and regeneration.

There may also be the following challenges for the direct regeneration of spent graphite. First, the cost of graphite is cheap (~2878 U.S. dollars), which makes the economic benefits of regenerated graphite too low, and the profit of regenerated graphite can be improved by converting the spent graphite to fast-charging graphite (~8640 U.S. dollars). Second, the spent graphite obtained from the factory contains

impurities, which is similar to the challenges encountered by the obtained cathode materials, which also requiring advanced separation technologies.

3. At present, the structural analysis of degraded cathode materials mainly relies on some basic characterization methods such as TEM, XPS, SEM, etc. More advanced characterization methods such as scanning electrochemical cell microscopy (SECM, which is an analytical technique that can be used to monitor electrochemical activity of a surface [206]), scanning transmission X-ray microscopy (STXM, an imaging technique that creates micron-scale images of a specimen's thin slice by systematically scanning it with a finely focused X-ray beam [207]), continuous rotation electron diffraction (cRED, which is suitable to obtain structural information of crystals smaller than 1 μm), neutron diffraction (ND, ND is a crystallographic technique utilized for the precise elucidation of the atomic and/or magnetic ordering within materials. [208]), nuclear magnetic resonance (NMR, which provides important structural information for a wide variety of materials), Kelvin probe force microscopy (KPFM, a microscopy technique that facilitates nanoscale mapping of the surface potential across a wide variety of material surfaces [209]), angle resolved photoelectron spectroscopy (ARPES, an advanced analytical method that allows for direct examination of the electronic structure [210]), and resonant inelastic X-ray scattering (RIXS, a spectroscopic technique that has proven instrumental in probing the electronic and magnetic excitations within materials [211]) are helpful in the analysis of failure mechanisms of cathode and explore novel and more effective direct repair methods.

4. Taking the direct regeneration of ternary cathode materials as an example, researchers can directly repair the spent ternary cathode materials in a variety of ways, including solution-based hydrothermal relithiation method and molten salt relithiation based on solid-state sintering. The method of hydrothermal relithiation is very challenging to achieve large-scale production because it is necessary to lithiate the spent cathodes under high pressure, [52,90,212] and the conditions of lithium replenishment are relatively extreme. Although molten salt relithition can realize the repair of the spent cathodes under normal pressure, according to previously reported literature, the amount of Li salt used is often greater than the amount of lithium deficiency of the spent cathode

materials to provide a lithium-rich environment in the process of direct regenerating the cathode, [51,87,128,213] which is easy to cause the waste of Li salt and reduce the recovery benefit. Therefore, we believe that in order to achieve large-scale production of regenerated materials, the relithiation of spent cathodes should be in the liquid phase environment at low temperature (<200 °C) and ordinary pressure. For the method of lithium supplementation at low temperature and normal pressure, sufficient contact between the spent cathode and the Li salt can be realized, and the concentration difference between the concentration of Li in the solution and the Li content of the spent cathodes can be used to automatically adjust the amount of relithiation of the spent cathode materials under the condition of the liquid phase. The above method can completely avoid the disadvantages of hydrothermal and molten salt relithiation.

In general, direct regeneration indeed represents a significant future direction for battery recycling. However, several key points are worth considering:

1. One major issue in current battery recycling is the lack of a comprehensive traceability system. It's challenging to identify the actual degraded state of recycled batteries, which greatly affects subsequent recycling processes, and the battery passport system could be a significant advancement in promoting this traceability system.

2. In practice, the removal of impurities in electrode materials is important for direct regeneration. For the direct regeneration of batteries, the development of an efficient and environmentally friendly impurity removal technology is a very crucial step.

3. In addition, the direct regeneration technologies for new types of batteries such as silicon-carbon anode, high-nickel, lithium manganese iron phosphate, cobalt-free batteries, and even solid-state batteries are indeed areas that require further exploration. These technologies hold great potential for the future of battery recycling, and continued research and development in these areas could lead to significant advancements in the field of direct regeneration of new types of batteries.

Conclusion

In this review, we discuss in detail the microstructures of components in spent materials from LIBs, including cathode and anode materials, and Al and Cu current

collectors, and analyze the degradation mechanisms of materials during cycling by different characterization methods. Based on an adequate understanding of the failure structures of different cycled materials, we propose the direct regeneration mechanisms and methods of these spent materials. Additionally, we illustrate the challenges against large-scale direct recycling of spent LIBs and propose corresponding solutions. We mainly highlight the degradation mechanisms and defect types of different cathode and negative materials in the process of electrochemical cycling, which provides sufficient theoretical preparation for the direct regeneration of spent materials and paves the way for people to explore more effective direct regeneration methods.

Data Availability statement

Data available on request from the authors.

Acknowledgements

K.X. appreciates support from the National Natural Science Foundation of China (No. 22278329), the high-level innovation and entrepreneurship talent project of Qinchuangyuan (No. OCYRCXM-2022-308), and the State Key Laboratory for Electrical Insulation and Power Equipment (No. EIPE23125). K.J acknowledges the "Young Talent Support Plan" of Xi'an Jiaotong University and the China National Postdoctoral Program for Innovative Talents (BX20230291).

Competing interest statement:

The authors declare no competing interest.

Reference

1 Xu, P *et al.* A Materials Perspective on Direct Recycling of Lithium-Ion Batteries: Principles, Challenges and Opportunities. *Advanced Functional Materials* **33**, 2213168, (2023).

2 Ji, G. *et al.* Direct regeneration of degraded lithium-ion battery cathodes with a multifunctional organic lithium salt. *Nature Communications* **14**, 584, (2023).

3 Tran, M. K., Rodrigues, M.-T. F., Kato, K., Babu, G. & Ajayan, P. M. Deep eutectic solvents for cathode recycling of Li-ion batteries. *Nature Energy* **4**, 339-345, (2019).

4 Yu, J., Ma, B., Qiu, Z., Wang, C. & Chen, Y. Separation and Recovery of Valuable Metals from Ammonia Leaching Solution of Spent Lithium-Ion Batteries. *ACS Sustainable Chemistry & Engineering* **11**, 9738–9750, (2023).

5 Fan, M. *et al.* Increased residual lithium compounds guided design for green recycling of

spent lithium-ion cathodes. *Energy & Environmental Science* **14**, 1461-1468, (2021).

6 Fan, M. *et al.* In Situ Electrochemical Regeneration of Degraded $LiFePO_4$ Electrode with Functionalized Prelithiation Separator. *Advanced Energy Materials* **12**, 2103630, (2022).

7 Council Directive 91/157/EEC of 18 March 1991 on batteries and accumulators containing certain dangerous substances, http://data.europa.eu/eli/dir/1991/157/oj.

8 Act on the Promotion of Effective Utilization of Resources 1991, https://www.japaneselawtranslation.go.jp/en/laws/view/3819/en.

9 Fan, E. *et al.* Sustainable Recycling Technology for Li-Ion Batteries and Beyond: Challenges and Future Prospects. *Chemical Reviews* **120**, 7020-7063, (2020).

10 Neuhaus, L. The Electrifying Problem of Used Lithium Ion Batteries: Recommendations for Recycling and Disposal. *Environs*, **42**, 65−91(2019).

11 Resource Conservation and Recovery Act (RCRA), https://www.epa.gov/rcra.

12 Law for the Promotion of Utilization of Recyclable Resources 2015, https://www.en.recycle21.co.jp/glossary/3r-law/.

13 The Recycling Scheme for Compact Rechargeable Batteries in Japan - under the Act on the Promotion of Effective Utilization of Resources, https://www.oecd.org/environment/waste/EPR_Japan_battery.pdf.

14 Heo H, Jung M. Case study for OECD project on extended producer responsibility Republic of Korea. https://www.oecd.org/environment/waste/OECD_EPR_case_study_Korea_revised_140522.pdf.

15 Settlements KRI for H. 2016 Modularization of Korea's Development Experience: Waste Resources Management and Utilization Policies of Korea. https://www.thegpsc.org/sites/gpsc/files/waste_resources_management_and_utilization_policies_of_korea_english.pdf.

16 Directive 2006/66/EC of the European Parliament and of the Council of 6 September 2006 on batteries and accumulators and waste batteries and accumulators and repealing Directive 91/157/EEC (Text with EEA relevance). http://data.europa.eu/eli/dir/2006/66/oj.

17 Technical policy for the recycling of automotive products,2006, https://www.mee.gov.cn/ywgz/fgbz/bz/bzwb/wrfzjszc/200611/t20061120_96237.shtml.

18 Directive 2008/98/EC of the European Parliament and of the Council of 19 November 2008 on waste and repealing certain Directives (Text with EEA relevance), http://data.europa.eu/eli/dir/2008/98/oj.

19 Directive 2013/56/EU of the European parliament and the council, http://data.europa.eu/eli/dir/2013/56/oj.

20 Tang, Y., Zhang, Q., Li, Y., Wang, G. & Li, Y. Recycling mechanisms and policy suggestions for spent electric vehicles' power battery -A case of Beijing. *Journal of Cleaner Production*, **186**, 388-406.

21 Ministry of Ecology and Environment of the PRC. Technical policy for waste batteries pollution prevention and control, https://www.mee.gov.cn/gkml/hbb/bgg/201612/t20161228_378325.htm.

22 Building a European battery industry, https://www.eba250.com.

23 MIIT Industry and Information Technology, Recycling of traction battery used in electric vehicle—Test of residual capacity, 2017,

https://openstd.samr.gov.cn/bzgk/gb/newGbInfo?hcno=A62FD663BD4648CC1C026D8AEBCEE762.

24 MIIT Industry and Information Technology, Recycling of traction battery used in electric vehicle—Dismantling specification, 2017, https://openstd.samr.gov.cn/bzgk/gb/newGbInfo?hcno=6F377279B21A21DF3BC36069272F9970.

25 L Gaines, K Richa, J. Spangenberger Key issues for Li-ion battery recycling MRS. *Energy Sustain.*, **5**, 1-14, (2018).

26 California legislature. AB 2407- Recycling: lithium-ion vehicle batteries: advisory group. https://leginfo.legislature.ca.gov/faces/billStatusClient.xhtml?bill_id=201720180AB2407.

27 Ministry of Industry and Information Technology of the PRC. Pilot implementation plan for recycling and utilizing power batteries of new energy vehicles, http://www.gov.cn/xinwen/2018-03/05/content_5270958.htm.

28 Ministry of Industry and Information Technology of the PRC. Interim provisions on the traceability management of the recovery and utilization of power batteries for new energy. Vehicles, https://www.miit.gov.cn/jgsj/jns/gzdt/art/2020/art_c1a708247cc54b068ea60ceaff0b044d.html.

29 Ministry of Industry and Information Technology of the PRC. Industry standard conditions for the comprehensive utilization of waste power batteries for new energy vehicles, https://wap.miit.gov.cn/zwgk/zcwj/wjfb/gg/art/2020/art_c1073817285c4b26a9fb34ed75a2e69d.html.

30 Ministry of Industry and Information Technology of the PRC. Guide for construction and operation of service station for recycling of new energy vehicles power batteries, https://www.gov.cn/xinwen/2019-11/08/content_5450006.htm.

31 National Blueprint For Lithium Batteries 2021–2030. https://www.energy.gov/sites/default/files/2021-06/FCAB%20National%20Blueprint%20Lithium%20Batteries%200621_0.pdf.

32 S. Korean government announces K-battery development strategy 2021, https://www.donga.com/en/article/all/20210710/2783299/1.

33 Implementation of the Infrastructure Investment and Jobs Act 2021, https://www.federalregister.gov/documents/2021/11/18/2021-25286/implementation-of-the-infrastructure-investment-and-jobs-act.

34 Inflation Reduction Act of 2022, https://www.energy.gov/lpo/inflation-reduction-act-2022.

35 Notice of the coordinated and stable development of the lithium-ion battery industry chain and supply chain, https://www.gov.cn/zhengce/zhengceku/2022-11/20/content_5727976.htm.

36 Regulation (EU) 2023/1542 of the European Parliament and of the Council of 12 July 2023 concerning batteries and waste batteries, http://data.europa.eu/eli/reg/2023/1542/oj.

37 Accelerating the development of the Administrative Measures for the Recycling of Power Storage Batteries for New Energy Vehicles, https://wap.miit.gov.cn/xwdt/gxdt/ldhd/art/2023/art_643c641ae55849eabd329f8311bc964d.html.

38 Qin, Z. *et al.* A Ternary Molten Salt Approach for Direct Regeneration of $LiNi_{0.5}Co_{0.2}$

$Mn_{0.3}O_2$ Cathode. *Small* **18**, 2106719, (2022).

39 Jing, Q. *et al.* Direct Regeneration of Spent $LiFePO_4$ Cathode Material by a Green and Efficient One-Step Hydrothermal Method. *ACS Sustainable Chemistry & Engineering* **8**, 17622-17628, (2020).

40 Wang, J. *et al.* Efficient Extraction of Lithium from Anode for Direct Regeneration of Cathode Materials of Spent Li-Ion Batteries. *ACS Energy Letters* **7**, 2816-2824, (2022).

41 Makuza, B., Tian, Q., Guo, X., Chattopadhyay, K. & Yu, D. Pyrometallurgical options for recycling spent lithium-ion batteries: A comprehensive review. *Journal of Power Sources* **491**, 229622, (2021).

42 Zhou, M., Li, B., Li, J. & Xu, Z. Pyrometallurgical Technology in the Recycling of a Spent Lithium Ion Battery: Evolution and the Challenge. *ACS ES&T Engineering* **1**, 1369-1382, (2021).

43 Xin, C. *et al.* Potential Controllable Redox Couple for Mild and Efficient Lithium Recovery from Spent Batteries. *Angewandte Chemie International Edition* **62**, e202310435, (2023)

44 Xin, C. *et al.* A Selective Extraction of Transition Metals from Spent $LiNi_xCo_yMn_{1-x-y}O_2$ Cathode via Regulation of Coordination Environment. *Angewandte Chemie International Edition* **61**, e202202558, (2022).

45 Wang, T. *et al.* Direct Recycling of Spent NCM Cathodes through Ionothermal Lithiation. *Advanced Energy Materials* **10**, 2001204, (2020).

46 Xu, Z. *et al.* A novel clustering algorithm for grouping and cascade utilization of retired Li-ion batteries. *Journal of Energy Storage* **29**, 101303, (2020).

47 Yan, Z., Sattar, A. & Li, Z. Priority Lithium recovery from spent Li-ion batteries via carbothermal reduction with water leaching. *Resources, Conservation and Recycling* **192**, 106937 (2023).

48 Shi, P. *et al.* Efficient separation and recovery of lithium and manganese from spent lithium-ion batteries powder leaching solution. *Separation and Purification Technology* **309**, 123063 (2023).

49 Xu, P. *et al.* Efficient Direct Recycling of Lithium-Ion Battery Cathodes by Targeted Healing. *Joule* **4**, 2609-2626, (2020).

50 Jia, K. *et al.* Adaptable Eutectic Salt for the Direct Recycling of Highly Degraded generation of Spent Lithium-Ion Battery Cathodes. *Journal of the American Chemical Society* **145**, 7288-7300, (2023).

51 Qin, Z. *et al.* A Universal Molten Salt Method for Direct Upcycling of Spent Ni-rich Cathode towards Single-crystalline Li-rich Cathode. *Angewandte Chemie International Edition* **62**, e202218672, (2023).

52 Jia, K. *et al.* Long-Life Regenerated $LiFePO_4$ from Spent Cathode by Elevating the d-Band Center of Fe. *Advance Materials* **35**, 2208034, (2022).

53 Wang, J. *et al.* Sustainable upcycling of spent $LiCoO_2$ to an ultra-stable battery cathode at high voltage. *Nature Sustainability* **6**, 797–805 (2023).

54 Ji, Y. *et al.* Directly-Regenerated $LiCoO_2$ with a Superb Cycling Stability at 4.6 V. *Energy Storage Materials* **60**, 102801, (2023).

55 Fei, Z. *et al.* Dual-Function Regeneration of Waste Lithium Cobalt Oxide for Stable High Voltage Cycle Performance. *ACS Sustainable Chemistry & Engineering* **9**, 11194-11203, (2021).

56 Oh, J. *et al.* Overcharge-Induced Phase Heterogeneity and Resultant Twin-Like Layer Deformation in Lithium Cobalt Oxide Cathode for Lithium-Ion Batteries. *Advanced Science* **9**, 2203639, (2022).

57 Tan, H., Takeuchi, S., Bharathi, K. K., Takeuchi, I. & Bendersky, L. A. Microscopy Study of Structural Evolution in Epitaxial $LiCoO_2$ Positive Electrode Films during Electrochemical Cycling. *ACS Applied Materials & Interfaces* **8**, 6727-6735, (2016).

58 Zan, M. *et al.* Conformal Coating of a High-Voltage Spinel to Stabilize $LiCoO_2$ at 4.6 V. *ACS Applied Materials & Interfaces* **15**, 5326-5335, (2023).

59 Chen, S.-X. *et al.* Co/Li-dual-site doping towards $LiCoO_2$ as a high-voltage, fast-charging, and long-cycling cathode material. *Journal of Materials Chemistry A* **10**, 5295-5304, (2022).

60 Zhou, S. *et al.* Collaborative Regeneration of Structural Evolution for High-Performance of $LiCoO_2$ Materials from Spent Lithium-Ion Batteries. *ACS Applied Energy Materials* **4**, 12677-12687, (2021).

61 Mu, X. *et al.* Advanced characterization guiding rational design of regeneration protocol for spent-$LiCoO_2$. *Nano Energy* **112**, 108465, (2023).

62 Zhuang, Z. *et al.* Ultrahigh-Voltage $LiCoO_2$ at 4.7 V by Interface Stabilization and Band Structure Modification. *Advanced Materials* **35**, 2212059, (2023).

63 Huang, H. *et al.* Dextran Sulfate Lithium as Versatile Binder to Stabilize High-Voltage $LiCoO_2$ to 4.6 V. *Advanced Energy Materials* **11**, 2101864, (2021).

64 Jia, K. *et al.* Suppressed Lattice Oxygen Release via Ni/Mn Doping from Spent $LiNi_{0.5}Mn_{0.3}Co_{0.2}O_2$ toward High-Energy Layered-Oxide Cathodes. *Nano Letters* **22**, 8372–8380, (2022).

65 Wang, J. *et al.* Direct and green repairing of degraded $LiCoO_2$ for reuse in lithium-ion batteries. *National Science Review* **9**, nwac097, (2022).

66 Tan, J. *et al.* Electrochemically Driven Phase Transition in $LiCoO_2$ Cathode. *Materials* **14**, 242, (2021).

67 Tang D. *et al.*, Porosification and Fe^{3+} Intercalation of Spent $LiCoO_2$ as an Efficient Oxygen Evolution Electrocatalyst. *Industrial & Engineering Chemistry Research* **61**, 16453–16460, (2022).

68 Chen, J. *et al.* Structure/Interface Coupling Effect for High-Voltage $LiCoO_2$ Cathodes. *Advanced Materials* **34**, 2204845, (2022).

69 Liu, J. *et al.* Tuning Interphase Chemistry to Stabilize High-Voltage $LiCoO_2$ Cathode Material via Spinel Coating. *Angewandte Chemie International Edition* **61**, 2207000, (2022).

70 Yang, X. *et al.* Pushing Lithium Cobalt Oxides to 4.7 V by Lattice-Matched Interfacial Engineering. *Advanced Energy Materials* **12**, 2200197 (2022).

71 Xia, J. *et al.* Lanthanide Contraction Builds Better High-Voltage $LiCoO_2$ Batteries. *Advanced Functional Materials* **33**, 2212869, (2022).

72 Wang, J. *et al.* Direct conversion of degraded $LiCoO_2$ cathode materials into high-performance $LiCoO_2$: A closed-loop green recycling strategy for spent lithium-ion batteries. *Energy Storage Materials* **45**, 768-776, (2022).

73 Liu, H. *et al.* Intergranular Cracking as a Major Cause of Long-Term Capacity Fading of Layered Cathodes. *Nano Letters* **17**, 3452-3457, (2017).

74 Gao, Y., Li, Y., Li, J., Xie, H. & Chen, Y. Direct recovery of $LiCoO_2$ from the recycled lithium-ion batteries via structure restoration. *Journal of Alloys and Compounds* **845**, 156234, (2020).

75 Chen, S. *et al.* Renovation of $LiCoO_2$ with outstanding cycling stability by thermal treatment with Li_2CO_3 from spent Li-ion batteries. *Journal of Energy Storage* **8**, 262-273, (2016).

76 Nie, H. *et al.* $LiCoO_2$: recycling from spent batteries and regeneration with solid state synthesis. *Green Chemistry* **17**, 1276-1280, (2015).

77 Lahtinen, K., Rautama, E. L., Jiang, H., Rasanen, S. & Kallio, T. Reuse of $LiCoO_2$ Electrodes Collected from Spent Li-Ion Batteries after Electrochemical Re-Lithiation of the Electrode. *ChemSusChem* **14**, 2434-2444, (2021).

78 Yang, T. *et al.* An Effective Relithiation Process for Recycling Lithium-Ion Battery Cathode Materials. *Advanced Sustainable Systems* **4**, 1900088, (2019).

79 Zhang, L., Xu, Z. & He, Z. Electrochemical Relithiation for Direct Regeneration of $LiCoO_2$ Materials from Spent Lithium-Ion Battery Electrodes. *ACS Sustainable Chemistry & Engineering* **8**, 11596-11605, (2020).

80 Kim, D.-S. *et al.* Simultaneous separation and renovation of lithium cobalt oxide from the cathode of spent lithium ion rechargeable batteries. *Journal of Power Sources* **132**, 145-149, (2004).

81 Shi, Y., Chen, G. & Chen, Z. Effective regeneration of $LiCoO_2$ from spent lithium-ion batteries: a direct approach towards high-performance active particles. *Green Chemistry* **20**, 851-862, (2018).

82 Chen, Y. *et al.* Durable and Adjustable Interfacial Engineering of Polymeric Electrolytes for Both Stable Ni-Rich Cathodes and High-Energy Metal Anodes. *Advanced Materials* **35**, 2300982, (2023).

83 Lu, Y. *et al.* Ultrathin LiV_2O_4 Layers Modified $LiNi_{0.5}Co_{0.2}Mn_{0.3}O_2$ Single-Crystal Cathodes with Enhanced Activity and Stability. *Advanced Materials Interfaces* **6**, 1901368, (2019).

84 Jeong, M. *et al.* Strategic Approach to Diversify Design Options for Li-Ion Batteries by Utilizing Low-Ni Layered Cathode Materials. *Advanced Energy Materials* **12**, 2103052, (2021).

85 Jung, S.-K. *et al.* Understanding the Degradation Mechanisms of $LiNi_{0.5}Co_{0.2}Mn_{0.3}O_2$ Cathode Material in Lithium Ion Batteries. *Advanced Energy Materials* **4**, 1300787, (2014).

86 Zhu, H. *et al.* Strain Engineering of Ni-Rich Cathode Enables Exceptional Cyclability in Pouch-Type Full Cells. *Advanced Materials* **35**, 2209357, (2022).

87 Ma, J. *et al.* Adaptable Eutectic Salt for the Direct Recycling of Highly Degraded Layer Cathodes. *Journal of the American Chemical Society* **144**, 20306-20314, (2022).

88 Qin, Z. *et al.* Self-Reconstruction of Highly Degraded $LiNi_{0.8}Co_{0.1}Mn_{0.1}O_2$ Towards Stable Single-Crystalline Cathode. *Advanced Materials*, e2307091, doi:10.1002/adma.202307091 (2023).

89 Wang, D. *et al.* Intrinsic Role of Cationic Substitution in Tuning Li/Ni Mixing in High-Ni Layered Oxides. *Chemistry of Materials* **31**, 2731-2740, (2019).

90 Gupta, V. *et al.* Scalable Direct Recycling of Cathode Black Mass from Spent Lithium-Ion Batteries. *Advanced Energy Materials* **13**, 2203093, (2022).

91 Liu, X. *et al.* Organic Eutectic Salts-Assisted Direct Lithium Regeneration for Extremely Low State of Health Ni-Rich Cathodes. *Advanced Energy Materials*, 2302987 (2023).

92 Liu, W. *et al.* Nickel-rich layered lithium transition-metal oxide for high-energy lithium-ion batteries. *Angewandte Chemie International Edition* **54**, 4440-4457, (2015).

93 Wang, C., Liu, F., Kan, K., Zhao, P. & Xiong, C. Realization of a high voltage Ni rich layer $LiNi_{0.5}Co_{0.2}Mn_{0.3}O_2$ single crystalline cathode for LIBs by surface modification. *Ceramics International* **49**, 7956-7964, (2023).

94 Xu, G.-L. *et al.* Building ultraconformal protective layers on both secondary and primary particles of layered lithium transition metal oxide cathodes. *Nature Energy* **4**, 484-494, (2019).

95 Shi, Y., Zhang, M., Meng, Y. S. & Chen, Z. Ambient-Pressure Relithiation of Degraded $Li_xNi_{0.5}Co_{0.2}Mn_{0.3}O_2$ ($0 < x < 1$) via Eutectic Solutions for Direct Regeneration of Lithium-Ion Battery Cathodes. *Advanced Energy Materials* **9**, 1900454, (2019).

96 Shi, Y., Chen, G., Liu, F., Yue, X. & Chen, Z. Resolving the Compositional and Structural Defects of Degraded $LiNi_xCo_yMn_zO_2$ Particles to Directly Regenerate High-Performance Lithium-Ion Battery Cathodes. *ACS Energy Letters* **3**, 1683-1692, (2018).

97 Jiang, G. *et al.* Direct Regeneration of $LiNi_{0.5}Co_{0.2}Mn_{0.3}O_2$ Cathode from Spent Lithium-Ion Batteries by the Molten Salts Method. *ACS Sustainable Chemistry & Engineering* **8**, 18138-18147, (2020).

98 Fan, X. *et al.* A green, efficient, closed-loop direct regeneration technology for reconstructing of the $LiNi_{0.5}Co_{0.2}Mn_{0.3}O_2$ cathode material from spent lithium-ion batteries. *Journal of Hazardous Materials* **410**, 124610, (2021).

99 Chi, Z. *et al.* Direct regeneration method of spent $LiNi_{1/3}Co_{1/3}Mn_{1/3}O_2$ cathode materials via surface lithium residues. *Green Chemistry* **23**, 9099-9108, (2021).

100 Yue, L.-P. *et al.* Regeneration of degraded $LiNi_{0.5}Co_{0.2}Mn_{0.3}O_2$ from spent lithium ion batteries. *Ionics* **26**, 2757-2761, (2020).

101 Dong, H. *et al.* Single-Crystal Materials Regenerated and Modified by Spent NCM523 as a High-Voltage Stable Cycling Cathode Material. *ACS Sustainable Chemistry & Engineering* **10**, 11587-11596, (2022).

102 Yang, X. *et al.* Restoring Surface Defect Crystal of Li-Lacking $LiNi_{0.6}Co_{0.2}Mn_{0.2}O_2$ Material Particles toward More Efficient Recycling of Lithium-Ion Batteries. *ACS Sustainable Chemistry & Engineering* **9**, 16997-17006, (2021).

103 Meng, X. *et al.* Recycling of $LiNi_{1/3}Co_{1/3}Mn_{1/3}O_2$ cathode materials from spent lithium-ion batteries using mechanochemical activation and solid-state sintering. *Waste Management* **84**, 54-63, (2019).

104 Chen, Y. *et al.* Enhancing the high-voltage electrochemical performance of the $LiNi_{0.5}Co_{0.2}Mn_{0.3}O_2$ cathode materials via hydrothermal lithiation. *Journal of Materials Science* **53**, 2115-2126, (2017).

105 Guo, Y. *et al.* High reversibility of layered oxide cathode enabled by direct Re-generation. *Energy Storage Materials* **43**, 348-357, (2021).

106 Yu, X. *et al.* Achieving low-temperature hydrothermal relithiation by redox mediation for direct recycling of spent lithium-ion battery cathodes. *Energy Storage Materials* **51**, 54-62, (2022).

107 Sloop, S. E. *et al.* Cathode healing methods for recycling of lithium-ion batteries.

Sustainable Materials and Technologies **22**, e00113, (2019).

108 Deng, B., Zhou, Z., Wang, W. & Wang, D. Direct Recovery and Efficient Reutilization of Degraded Ternary Cathode Materials from Spent Lithium-Ion Batteries via a Homogeneous Thermochemical Process. *ACS Sustainable Chemistry & Engineering* **8**, 14022-14029, (2020).

109 Fan, M. *et al.* Structural Restoration of Degraded $LiFePO_4$ Cathode with Enhanced Kinetics Using Residual Lithium in Spent Graphite Anodes. *CCS Chemistry* **5**, 1189-1201, (2023).

110 Song, L. *et al.* Direct regeneration of waste $LiFePO_4$ cathode materials with a solid-phase method promoted by activated CNTs. *Waste Management* **157**, 141-148, (2023).

111 Yu, J., Wang, X., Zhou, M. & Wang, Q. A redox targeting-based material recycling strategy for spent lithium ion batteries. *Energy & Environmental Science* **12**, 2672-2677, (2019).

112 Liu, P. *et al.* Direct regeneration of spent $LiFePO_4$ cathode materials with pre-oxidation and V-doping. *Journal of Alloys and Compounds* **860**, 157909, (2021).

113 ang, T. *et al.* Direct regeneration of spent $LiFePO_4$ via a graphite prelithiation strategy. *Chem Commun (Camb)* **56**, 245-248, (2019).

114 Yang, Y., Liu, Z., Zhang, J., Chen, Y. & Wang, C. Economical and low-carbon regeneration of spent $LiFePO_4$ materials by hydrothermal relithiation. *Journal of Alloys and Compounds* **947**, 169660, (2023).

115 Wu, J. *et al.* Direct recovery: A sustainable recycling technology for spent lithium-ion battery. *Energy Storage Materials* **54**, 120-134, (2023).

116 Quilty, C. D. *et al.* Electron and Ion Transport in Lithium and Lithium-Ion Battery Negative and Positive Composite Electrodes. *Chem Reviews* **123**, 1327–1363, (2023).

117 Ren, X., Guo, J., Liu, R., Guo, H. & Liang, G. Are Fe-Li Antisite Defects Necessarily Detrimental to the Diffusion of Li^+ in $LiFePO_4$/C? *Journal of The Electrochemical Society* **169**, 120507, (2022).

118 Zeng, J. *et al.* $LiFePO_4$/carbon hybrids with fast Li-ion solid transfer capability obtained by adjusting the superheat temperature. *Journal of Alloys and Compounds* **803**, 998-1004, (2019).

119 Huang, X., He, X., Jiang, C., Tian, G. & Liu, Y. Reaction Mechanisms on Solvothermal Synthesis of Nano $LiFePO_4$ Crystals and Defect Analysis. *Industrial & Engineering Chemistry Research* **56**, 10648-10657, (2017).

120 Wheatcroft, L., Tran, T. D., Özkaya, D., Cookson, J. & Inkson, B. J. Visualization of the Delithiation Mechanisms in High-Voltage Battery Material $LiCoPO_4$. *ACS Applied Energy Materials* **5**, 196-206, (2022).

121 Susanto, D. *et al.* Anionic Redox Activity as a Key Factor in the Performance Degradation of $NaFeO_2$ Cathodes for Sodium Ion Batteries. *Chemistry of Materials* **31**, 3644-3651, (2019).

122 Wang, W. *et al.* Probing Hybrid $LiFePO_4$/$FePO_4$ Phases in a Single Olive $LiFePO_4$ Particle and Their Recovering from Degraded Electric Vehicle Batteries. *Nano Letters* **23**, 7485–7492, (2023).

123 Kobayashi, S., Kuwabara, A., Fisher, C. A. J. & Ikuhara, Y. Atomic-Scale Analysis of Biphasic Boundaries in the Lithium-Ion Battery Cathode Material $LiFePO_4$. *ACS Applied Energy Materials* **3**, 8009-8016, (2020).

124 Li, W. *et al.* Ultrathin and uniform carbon-layer-coated hierarchically porous $LiFePO_4$

microspheres and their electrochemical performance. *The Journal of Supercritical Fluids* **116**, 164-171, (2016).

125 Lai, A. *et al.* Self-restriction to form in-situ N,P co-doped carbon-coated $LiFePO_4$ nanocomposites for high-performance lithium ion batteries. *Electrochimica Acta* **414**, 140161, (2022).

126 Li, Y. *et al.* High performance of $LiFePO_4$ with nitrogen and phosphorus dual-doped carbon layer for lithium-ion batteries. *Journal of Alloys and Compounds* **890**, 161617, (2022).

127 Qi, C. *et al.* Environmental-friendly low-cost direct regeneration of cathode material from spent $LiFePO_4$. *Journal of Alloys and Compounds* **924**, 166612, (2022).

128 Liu, X. *et al.* Direct Regeneration of Spent Lithium Iron Phosphate via a Low-Temperature Molten Salt Process Coupled with a Reductive Environment. *Industrial & Engineering Chemistry Research* **61**, 3831–3839, (2022).

129 Lee, J., Zhou, W., Idrobo, J. C., Pennycook, S. J. & Pantelides, S. T. Vacancy-driven anisotropic defect distribution in the battery-cathode material $LiFePO_4$. *Physical Review Letters* **107**, 085507, (2011).

130 Bai, P., Cogswell, D. A. & Bazant, M. Z. Suppression of phase separation in $LiFePO_4$ nanoparticles during battery discharge. *Nano Letters* **11**, 4890-4896, (2011).

131 Park, K.-Y. *et al.* Anti-Site Reordering in $LiFePO_4$: Defect Annihilation on Charge Carrier Injection. *Chemistry of Materials* **26**, 5345-5351, (2014).

132 Chen, J. *et al.* Environmentally friendly recycling and effective repairing of cathode powders from spent $LiFePO_4$ batteries. *Green Chemistry* **18**, 2500-2506, (2016).

133 Li, J., Wang, Y., Wang, L., Liu, B. & Zhou, H. A facile recycling and regeneration process for spent $LiFePO_4$ batteries. *Journal of Materials Science: Materials in Electronics* **30**, 14580-14588, (2019).

134 Liang, Q. *et al.* Recycling and crystal regeneration of commercial used $LiFePO_4$ cathode materials. *Electrochimica Acta* **330**, 135323 (2020).

135 Sun, Q. *et al.* Resynthesizing $LiFePO_4$/C materials from the recycled cathode via a green full-solid route. *Journal of Alloys and Compounds* **818**, 153292, (2020).

136 Li, X., Zhang, J., Song, D., Song, J. & Zhang, L. Direct regeneration of recycled cathode material mixture from scrapped $LiFePO_4$ batteries. *Journal of Power Sources* **345**, 78-84, (2017).

137 Peng, D. *et al.* Efficient regeneration of retired $LiFePO_4$ cathode by combining spontaneous and electrically driven processes. *Green Chemistry* **24**, 4544-4556, (2022).

138 Tang, X. *et al.* Effective regeneration of scrapped $LiFePO_4$ material from spent lithium-ion batteries. *Journal of Materials Science* **55**, 13036-13048, (2020).

139 Tao, R. *et al.* In situ reduction of cathode material by organics and anode graphite without additive to recycle spent electric vehicle $LiMn_2O_4$ batteries. *Journal of Power Sources* **520**, 230827, (2022).

140 Mandal, D., Bharti, L., Biswas, S. & Chandra, A. Graphene decorated $LiMn_2O_4$ electrode material for hybrid type energy storage devices. *Energy Storage* **5**, e373, (2022).

141 Gao, H. *et al.* Efficient Direct Recycling of Degraded $LiMn_2O_4$ Cathodes by One-Step Hydrothermal Relithiation. *ACS Applied Materials & Interfaces* **12**, 51546-51554, (2020).

142 Wu, C. *et al.* Cost-effective recycling of spent $LiMn_2O_4$ cathode via a chemical lithiation strategy. *Energy Storage Materials* **55**, 154-165, (2023).

143 Lin, J. *et al.* A green repair pathway for spent spinel cathode material: Coupled mechanochemistry and solid-phase reactions. *eScience* **3**, 100110 (2023).

144 Palaniyandy, N., Rambau, K., Musyoka, N. & Ren, J. A Facile Segregation Process and Restoration of $LiMn_2O_4$ Cathode Material From Spent Lithium-Ion Batteries. *Journal of The Electrochemical Society* **167**, 090510, (2020).

145 Lin, J. *et al.* Sustainable Upcycling of Spent Lithium-Ion Batteries Cathode Materials: Stabilization by In Situ Li/Mn Disorder. *Advanced Energy Materials* **12**, 2201174, (2022).

146 Zhang, J. *et al.* Interfacial Design for a 4.6 V High-Voltage Single-Crystalline $LiCoO_2$ Cathode. *Advanced Materials* **34**, 2108353, (2022).

147 Tian, F. *et al.* Understanding high-temperature cycling-induced crack evolution and associated atomic-scale structure in a Ni-rich $LiNi_{0.8}Co_{0.1}Mn_{0.1}O_2$ layered cathode material. *Nano Energy* **98**, 107222, (2022).

148 Meng, Q., Duan, J., Zhang, Y. & Dong, P. Novel efficient and environmentally friendly recovering of high performance nano-$LiMnPO_4$/C cathode powders from spent $LiMn_2O_4$ batteries. *Journal of Industrial and Engineering Chemistry* **80**, 633-639, (2019).

149 Wang, J., Xu, Y., Niu, Y., Liu, Y. & Yao, X. Lithium-Ion Conductivity Epitaxial Layer Contributing to the Structure and Cycling Stability of $LiMn_2O_4$ Cathodes. *ACS Sustainable Chemistry & Engineering* **11**, 5408-5419, (2023).

150 Chen, T., Yang, J., Barroso-Luque, L. & Ceder, G. Removing the Two-Phase Transition in Spinel $LiMn_2O_4$ through Cation Disorder. *ACS Energy Letters* **8**, 314-319, (2022).

151 Hou, X. *et al.* Specific countermeasures to intrinsic capacity decline issues and future direction of $LiMn_2O_4$ cathode. *Energy Storage Materials* **57**, 577-606, (2023).

152 Liu, T. *et al.* Correlation between manganese dissolution and dynamic phase stability in spinel-based lithium-ion battery. *Nature Communications* **10**, 4721, (2019).

153 Wang, H. & Whitacre, J. F. Direct Recycling of Aged $LiMn_2O_4$ Cathode Materials used in Aqueous Lithium-ion Batteries: Processes and Sensitivities. *Energy Technology* **6**, 2429-2437, (2018).

154 Sun, C. *et al.* 50C Fast-Charge Li-Ion Batteries using a Graphite Anode. *Advanced Materials* **34**, 2206020, (2022).

155 Shen, Y. *et al.* Achieving Desirable Initial Coulombic Efficiencies and Full Capacity Utilization of Li-Ion Batteries by Chemical Prelithiation of Graphite Anode. *Advanced Functional Materials* **31**, 2101181, (2021).

156 Li, P., Kim, H., Myung, S.-T. & Sun, Y.-K. Diverting Exploration of Silicon Anode into Practical Way: A Review Focused on Silicon-Graphite Composite for Lithium Ion Batteries. *Energy Storage Materials* **35**, 550-576, (2021).

157 Da, H. *et al.* Greatly recovered electrochemical performances of regenerated graphite anode enabled by an artificial PMMA solid electrolyte interphase layer. *Energy Storage Materials* **56**, 457-467, (2023).

158 Da, H. *et al.* Epitaxial Regeneration of Spent Graphite Anode Material by an Eco-friendly In-Depth Purification Route. *ACS Sustainable Chemistry & Engineering* **9**, 16192-16202, (2021).

159 Jayasree, S. S. *et al.* Energy efficient lattice and surface chemical regeneration of graphite from failed Li-ion batteries and its use as ultra-long cycling Na-ion battery anodes. *Resources, Conservation and Recycling* **190**, 106841, (2023).

160 Yang, D. *et al.* An efficient recycling strategy to eliminate the residual “impurities” while heal the damaged structure of spent graphite anodes. *Green Energy & Environment*, doi:10.1016/j.gee.2022.11.003, (2022).

161 Natarajan, S. & Aravindan, V. An Urgent Call to Spent LIB Recycling: Whys and Wherefores for Graphite Recovery. *Advanced Energy Materials* **10**, 2002238, (2020).

162 Qiao, Y. *et al.* Recycling of graphite anode from spent lithium-ion batteries: Advances and perspectives. *EcoMat* **5**, e12321, (2023).

163 Huang, W., Feng, X., Han, X., Zhang, W. & Jiang, F. Questions and Answers Relating to Lithium-Ion Battery Safety Issues. *Cell Reports Physical Science* **2**, 100285, (2021).

164 Yan, C., Yuan, H., Park, H. S. & Huang, J.-Q. Perspective on the critical role of interface for advanced batteries. *Journal of Energy Chemistry* **47**, 217-220, (2020).

165 Lai, Y. *et al.* Recovery and regeneration of anode graphite from spent lithium-ion batteries through deep eutectic solvent treatment: Structural characteristics, electrochemical performance and regeneration mechanism. *Chemical Engineering Journal* **457**, 141196, (2023).

166 Lei, Y. *et al.* Unveiling the influence of electrode/electrolyte interface on the capacity fading for typical graphite-based potassium-ion batteries. *Energy Storage Materials* **24**, 319-328, (2020).

167 Lu, D., Xu, M., Zhou, L., Garsuch, A. & Lucht, B. L. Failure Mechanism of Graphite/$LiNi_{0.5}Mn_{1.5}O_4$ Cells at High Voltage and Elevated Temperature. *Journal of The Electrochemical Society* **160**, A3138-A3143, (2013).

168 Sethuraman, V. A., Hardwick, L. J., Srinivasan, V. & Kostecki, R. Surface structural disordering in graphite upon lithium intercalation/deintercalation. *Journal of Power Sources* **195**, 3655-3660, (2010).

169 Zhang, S. S., Ma, L., Allen, J. L. & Read, J. A. Stabilizing Capacity Retention of Li-Ion Battery in Fast-Charge by Reducing Particle Size of Graphite. *Journal of The Electrochemical Society* **168**, 040519, (2021).

170 Luo, J. *et al.* Recycle spent graphite to defect-engineered, high-power graphite anode. *Nano Research* **16**, 4240–4245, (2022).

171 He, K., Zhang, Z. Y. & Zhang, F. S. Synthesis of graphene and recovery of lithium from lithiated graphite of spent Li-ion battery. *Waste Management* **124**, 283-292, (2021).

172 Xu, Y.-j. *et al.* The regeneration of graphite anode from spent lithium-ion batteries by washing with a nitric acid/ethanol solution. *New Carbon Materials* **37**, 1011-1020, (2022).

173 Rinkel, B. L. D., Vivek, J. P., Garcia-Araez, N. & Grey, C. P. Two electrolyte decomposition pathways at nickel-rich cathode surfaces in lithium-ion batteries. *Energy & Environmental Science* **15**, 3416-3438, (2022).

174 Meda, U. S., Lal, L., M, S. & Garg, P. Solid Electrolyte Interphase (SEI), a boon or a bane for lithium batteries: A review on the recent advances. *Journal of Energy Storage* **47**, 103564, (2022).

175 McShane, E. J. *et al.* Multimodal quantification of degradation pathways during extreme fast charging of lithium-ion batteries. *Journal of Materials Chemistry A* **10**, 23927-23939, (2022).

176 S. Klein *et al.* Understanding the Outstanding High-Voltage Performance of NCM523||Graphite Lithium Ion Cells after Elimination of Ethylene Carbonate Solvent

from Conventional Electrolyte. *Advanced Energy Materials* **11**, 2003738, (2021).

177 Teresa Insinna *et al.* Graphite Anodes for Li-Ion Batteries: An Electron Paramagnetic Resonance Investigation. *Chemistry of Materials* **35**, 5497–5511, (2023)

178 Geng, Z. *et al.* Separation and recovery of graphite from spent lithium–ion batteries for synthesizing micro-expanded sorbents. *New Journal of Chemistry* **46**, 20250-20259, (2022).

179 Li, J. *et al.* Hydrometallurgical enhanced liberation and recovery of anode material from spent lithium-ion batteries. *Waste Management* **126**, 517-526, (2021).

180 Yang, X. *et al.* A novel route to constructing high-efficiency lithium sulfur batteries with spent graphite as the sulfur host. *Carbon* **199**, 215-223, (2022).

181 Mousa, E., Hu, X. & Ye, G. Effect of Graphite on the Recovery of Valuable Metals from Spent Li-Ion Batteries in Baths of Hot Metal and Steel. *Recycling* **7**, 5, (2022).

182 Markey, B. *et al.* Effective Upcycling of Graphite Anode: Healing and Doping Enabled Direct Regeneration. *Journal of The Electrochemical Society* **167**, 160511, (2020).

183 Yi, C. *et al.* Technology for recycling and regenerating graphite from spent lithium-ion batteries. *Chinese Journal of Chemical Engineering* **39**, 37-50, (2021).

184 Chen, Q., Huang, L., Liu, J., Luo, Y. & Chen, Y. A new approach to regenerate high-performance graphite from spent lithium-ion batteries. *Carbon* **189**, 293-304, (2022).

185 Liu, J. *et al.* Critical strategies for recycling process of graphite from spent lithium-ion batteries: A review. *Science of the Total Environment* **816**, 151621, (2022).

186 Li, Y. *et al.* Regeneration of anode materials from complex graphite residue in spent lithium-ion battery recycling process. *Green Chemistry* **24**, 9315-9328, (2022).

187 Ma, X., Chen, M., Chen, B., Meng, Z. & Wang, Y. High-Performance Graphite Recovered from Spent Lithium-Ion Batteries. *ACS Sustainable Chemistry & Engineering* **7**, 19732-19738, (2019).

188 Chen, W. *et al.* Flash Recycling of Graphite Anodes. *Advanced Materials* **35**, 2207303, (2023).

189 Zhang, H. *et al.* Transient and dry recycling of battery materials with negligible carbon footprint and roll-to-roll scalability. *Energy & Environmental Science* **16**, 2561-2571, (2023).

190 Gao, Y. *et al.* Graphite Recycling from the Spent Lithium-Ion Batteries by Sulfuric Acid Curing–Leaching Combined with High-Temperature Calcination. *ACS Sustainable Chemistry & Engineering* **8**, 9447-9455, (2020).

191 Natarajan, S., Akshay, M. & Aravindan, V. Recycling/Reuse of Current Collectors from Spent Lithium-Ion Batteries: Benefits and Issues. *Advanced Sustainable Systems* **6**, 2100432, (2022).

192 Khatibi, H. *et al.* Recycling and Reusing Copper and Aluminum Current-Collectors from Spent Lithium-Ion Batteries. *Energies* **15**, 9069, (2022).

193 Chernyaev, A. *et al.* The efficiency of scrap Cu and Al current collector materials as reductants in LIB waste leaching. *Hydrometallurgy* **203**, 105608, (2021).

194 Sommerville, R., Shaw-Stewart, J., Goodship, V., Rowson, N. & Kendrick, E. A review of physical processes used in the safe recycling of lithium ion batteries. *Sustainable Materials and Technologies* **25**, e00197, (2020).

195 Neumann, J. *et al.* Recycling of Lithium-Ion Batteries—Current State of the Art, Circular Economy, and Next Generation Recycling. *Advanced Energy Materials* **12**, 2102917,

(2022).

196 Natarajan, S. *et al.* A new route for the recycling of spent lithium-ion batteries towards advanced energy storage, conversion, and harvesting systems. *Nano Energy* **101**, 107595, (2022).

197 Zhu, P. *et al.* Direct reuse of aluminium and copper current collectors from spent lithium-ion batteries. *Green Chemistry* **25**, 3503-3514, (2023).

198 Shu, J. *et al.* Comparative study on surface behaviors of copper current collector in electrolyte for lithium-ion batteries. *Electrochimica Acta* **56**, 3006-3014, (2011).

199 Lin, L. *et al.* Epitaxial Induced Plating Current-Collector Lasting Lifespan of Anode-Free Lithium Metal Battery. *Advanced Energy Materials* **11**, 2003709 (2021).

200 Jeong, H., Jang, J. & Jo, C. A review on current collector coating methods for next-generation batteries. *Chemical Engineering Journal* **446**, 136860 (2022).

201 Myung, S.-T., Sasaki, Y., Sakurada, S., Sun, Y.-K. & Yashiro, H. Electrochemical behavior of current collectors for lithium batteries in non-aqueous alkyl carbonate solution and surface analysis by ToF-SIMS. *Electrochimica Acta* **55**, 288-297, (2009).

202 Myung, S.-T., Hitoshi, Y. & Sun, Y.-K. Electrochemical behavior and passivation of current collectors in lithium-ion batteries. *Journal of Materials Chemistry* **21**, 9891-9911, (2011).

203 Subramanyan, K., Akshay, M., Lee, Y. S. & Aravindan, V. Fabrication of Na-Ion Full-Cells using Carbon-Coated $Na_3V_2(PO_4)_2O_2F$ Cathode with Conversion Type CuO Nanoparticles from Spent Li-Ion Batteries. *Small Methods* **6**, 2200257, (2022).

204 Yu, J. *et al.* Mechanochemical upcycling of spent $LiCoO_2$ to new $LiNi_{0.80}Co_{0.15}Al_{0.05}O_2$ battery: An atom economy strategy. *Proceedings of the National Academy of Sciences of the United States of America* **120**, e2217698120, (2023).

205 Xing, C. *et al.* Aluminum Impurity from Current Collectors Reactivates Degraded NCM Cathode Materials toward Superior Electrochemical Performance. *ACS Nano* **17**, 3194-3203, (2023).

206 Zhang, H. *et al.* Angle-resolved photoemission spectroscopy. *Nature Reviews Methods Primers* **2**, 54, (2022).

207 Zhang, W. *et al.* Chemical-state distributions in charged $LiCoO_2$ cathode particles visualized by soft X-ray spectromicroscopy. *Scientific Reports* **13**, 4639, (2023).

208 Liu, H. *et al.* Operando Lithium Dynamics in the Li-Rich Layered Oxide Cathode Material via Neutron Diffraction. *Advanced Energy Materials* **6**, 1502143, (2016).

209 Wu, J. *et al.* Multi-characterization of $LiCoO_2$ cathode films using advanced AFM-based techniques with high resolution. *Scientific Reports* **7**, 11164, (2017).

210 Wang, Y. *et al.* Directional Manipulation of Electron Transfer by Energy Level Engineering for Efficient Cathodic Oxygen Reduction. *Nano Letters* **22**, 6622-6630, (2022).

211 Hu, E. *et al.* Oxygen-redox reactions in $LiCoO_2$ cathode without O–O bonding during charge-discharge. *Joule* **5**, 720-736, (2021).

212 Gao, H. *et al.* Efficient Direct Recycling of Degraded $LiMn_2O_4$ Cathodes by One-Step Hydrothermal Relithiation. *ACS Applied Materials & Interfaces* **12**, 51546-51554, (2020).

213 Qian, G. *et al.* Value-creating upcycling of retired electric vehicle battery cathodes. *Cell Reports Physical Science* **3**, 100741 (2022).